

1 Title: Playing with the ploidy level enables to switch on and off the strict recombination control
2 even in the vicinity of *Brassica* centromeres
3

4 Authors: Franz Boideau¹, Virginie Huteau¹, Anael Brunet¹, Loeiz Maillet¹, Olivier Coriton¹,
5 Gwenn Trotoux¹, Maryse Lodé-Taburel¹, Gwenaëlle Deniot¹, Frédérique Eber¹, Marie Gilet¹,
6 Julien Boutte¹, Jérôme Morice¹, Cyril Falentin¹, Olivier Martin^{2,3}, Matthieu Falque⁴, Anne-Marie
7 Chèvre^{1*}, Mathieu Rousseau-Gueutin^{1*}

8 * : corresponding authors

9 Affiliations :

10 ¹ IGEPP, INRAE, Institut Agro, Université de Rennes, 35650 Le Rheu, France

11 ² Université Paris-Saclay, CNRS, INRAE, Univ Evry, Institute of Plant Sciences Paris-Saclay
12 (IPS2), 91405, Orsay, France

13 ³ Université de Paris, CNRS, INRAE, Institute of Plant Sciences Paris-Saclay (IPS2), 91405,
14 Orsay, France

15 ⁴ Université Paris-Saclay, INRAE, CNRS, AgroParisTech, GQE - Le Moulon, 91190 Gif-sur-
16 Yvette, France
17

18 **Abstract**

19 Meiotic recombination is a key biological process in plant evolution and breeding, as it generates
20 novel genetic diversity at each generation. However, due to its importance in chromosome
21 segregation and genomic stability, crossovers are highly regulated in both frequency and
22 distribution. We previously demonstrated that this strict regulation is not a fatality and that it can
23 be naturally modified (3.6-fold increased frequency and altered distribution) in an allotriploid
24 *Brassica* hybrid ($2n=3x=29$; AAC), resulting from a cross between *B. napus* ($2n=4x=38$; AACC)
25 and *B. rapa* ($2n=2x=20$; AA). Taking advantage of the recently updated *Brassica napus* genome
26 assembly, which now includes the pericentromeric regions, we unambiguously demonstrated that
27 crossovers occur in these normally cold regions in allotriploids, with the presence of crossovers
28 as close as 375 kb from the centromere. We deciphered that this modified recombination
29 landscape (both frequency and distribution) can be maintained in successive generations of
30 allotriploidy, with even a slight increase of crossover frequency. We also showed that this
31 deregulated meiotic behavior may revert back to a strictly regulated one when recovering an
32 allotetraploid progeny in the second generation. Overall, we provide here for the first time a
33 practical and natural way to switch on and off the tight recombination control in a polyploid crop.
34 We also discuss the potential role of this modified regulation of recombination in polyploid
35 speciation success.

36

37 **Introduction**

38 Meiotic recombination is a key biological process in sexually reproducing eukaryotes, as it both
39 ensures the faithful segregation of chromosomes and generates a novel genetic diversity at each
40 generation. It is initiated in prophase I by the formation of Double-Strand Breaks (DSBs). From
41 about 250 DSBs occurring at each meiosis in *Arabidopsis*, only a few (~ 10) will form crossovers
42 (COs), the other giving rise to non-crossovers (Mercier et al. 2015). These COs belong to two
43 classes (I and II) depending on the meiotic proteins involved. Most formed COs (70-85%) derive
44 from the Class I, which is controlled by proteins of the ZMM group (ZYP1, ZIP2, ZIP3, ZIP4,
45 MSH4, MSH5 and MER3, MutL γ complex with MLH1/MLH3 and HEI10). These COs are
46 subject to interference, a process that prevents the formation of two close-by class I COs. The few
47 remaining COs (15-30%) derive from the Class II, which depends mainly on the MUS81 pathway
48 and are interference insensitive (Mercier et al. 2015).

49 In most cases, meiotic recombination is strictly regulated, with one obligate CO per pair of
50 homologous chromosomes to ensure the proper segregation of chromosomes, but rarely more
51 than three (Mercier et al. 2015). Additionally, the distribution of COs is not homogeneous along
52 the chromosomes and presents a species-specific pattern: one can have a “U” distribution with its
53 minimum at the centromere as in *Arabidopsis thaliana*, or a rather linear increase of CO rate from
54 the centromere to the telomere as in several crop species such as wheat, maize, barley, or oilseed
55 rape (see Wang and Copenhaver 2018 for review). In most organisms, it has been observed that
56 80% of the COs were concentrated in about 25% of the genome (Choi et al. 2013, Darrier et al.
57 2017). This uneven distribution of COs is associated with the global chromatin organization on
58 the chromosome. Indeed, COs mainly occur in open chromatin, which harbors a low nucleosome
59 density, a low DNA methylation and is enriched in H3K4me3 (Choi et al. 2013, 2015, Marand et
60 al., 2017, Lian et al. 2022). In contrast, COs are largely suppressed in the regions close to the
61 centromeres, corresponding to the chromosomal region where the kinetochore platform
62 assembles to allow the attachment of the spindle and the segregation of chromosomes at the
63 opposite pole of meiocytes (McKinley and Cheeseman 2016). These centromeric regions are
64 heterochromatic, repeat-rich, dense in nucleosomes, heavily methylated and enriched in
65 H3K9me2 (Yelina et al. 2012, Underwood et al. 2018). Despite this tight control of meiotic
66 recombination in most organisms, some variations may exist within a species, influencing the

67 species evolution and adaptation (Coop and Przeworski, 2022). These differences can be the
68 result of allele or copy number variations of certain meiotic genes, such as *HEI10* (Ziolkowski et
69 al. 2017), but also can be related to the sex (Lenormand and Dutheil, 2005). Indeed, different CO
70 landscapes have been observed between male and female meiosis in several species, a
71 phenomenon referred as heterochiasmy (Sardell and Kirkpatrick, 2020, Capilla-Perez et al. 2021,
72 Cai et al. 2023). Within the last ten years, several methods have emerged to greatly increase the
73 number of COs per meiosis, either by over-expressing pro-COs genes such as *HEI10* (Ziolkowski
74 et al. 2017), or by knocking-out (KO) anti-COs genes (e.g. *FANCM*, *FANCC*, *RECQ4*, *FIGL1* or
75 *ZYP1*: Crismani et al. 2012, Séguéla-Arnaud et al. 2015, Girard et al. 2015, Durand et al. 2022,
76 Singh et al. 2023, Capilla-Perez et al. 2024) or by combining both approaches (Serra et al. 2018).
77 As an example, the recent overexpression of the pro-COs HEI10 protein combined with the KO
78 of the *ZYP1* gene involved in the synaptonemal complex gave rise to a massive increase of COs,
79 but only in regions where COs normally occur (Durand et al. 2022). To date, very few cases have
80 led to an increase of CO numbers near the centromeric regions. Most of them were obtained
81 when performing a K.O. of genes involved in epigenetic marks. As an example, the loss of CG
82 methylation via the KO of *MET1* (DNA hypomethylated methyltransferase 1) or *DDMI*
83 (decreased DNA methylation 1) in Arabidopsis altered the CO distribution, with an increased
84 COs number around the centromeres but also a decrease in pericentromeric regions (Melamed-
85 Bessudo and Levy, 2012, Yelina et al. 2012). Similarly, the disruption of Arabidopsis H3K9me2
86 and non-CG DNA methylation pathways (via the mutation of *KYP/SUVH5/SUVH6*, and *CMT3*),
87 slightly increased meiotic recombination in proximity to the centromeres, including
88 pericentromeres (Underwood et al., 2018). A third factor affecting recombination corresponds to
89 the ploidy level. In the case of allopolyploid species, corresponding to the presence of at least two
90 different genomes in the same nucleus, it has been observed in some species a 2-fold increase of
91 recombination rate, as exemplified in *Gossypium* (Brubaker et al. 1999, Desai et al. 2006),
92 Arabidopsis (Pecinka et al. 2011), Brassicoraphanus (Park et al. 2020), or wheat (Wan et al.,
93 2021, Yang et al. 2022). In *Brassica*, it has been found that allotriploidy increased by 3.5-fold the
94 homologous recombination compared to its diploid and even its allotetraploid counterpart, with
95 also 1.7 times more recombination in female meiosis compared to the male meiosis (Pelé et al.
96 2017). Interestingly, allotriploids present a modified recombination pattern, independently of the
97 sex of meiosis (Leflon et al. 2010, Pelé et al. 2017, Boideau et al. 2021). Within such allotriploid

98 *Brassica* hybrids ($2n=3x=29$; AAC) deriving from a cross between *B. napus* ($2n=4x=38$; AACC)
99 and *B. rapa* ($2n=2x=20$; AA), the A chromosomes pair as ten bivalents, whereas the remaining
100 nine C chromosomes remain as univalent at metaphase I and segregate randomly within gametes
101 (Leflon et al. 2006). It has been proposed that the presence of univalents may cause the nucleus to
102 linger in a recombination active state, resulting in an increase CO number and in a modified
103 distribution in the remaining chromosomes that are correctly synapsed (Martinez-Perez and
104 Moore, 2008). Until recently, it remained unknown if this unique recombination was specific to
105 *Brassica* and allotriploids. However, a similar study had been performed in a monocotyledon
106 pentaploid wheat, deriving from a cross between a hexaploid wheat (*Triticum aestivum*,
107 $2n=6x=42$, AABBDD) and a tetraploid wheat (*Triticum turgidum*, $2n=4x=28$). That study also
108 found a CO increase (3 to 4-fold) between either A or B homologous chromosomes and a modified
109 distribution (Yang et al. 2022). These different results suggest that this modified recombination
110 pattern observed in both a monocotyledon and dicotyledon may be used to efficiently improve
111 the genetic diversity and breeding of many polyploid crops, such as wheat, cotton, oilseed rape,
112 coffee and strawberry (Leitch and Leitch, 2008).

113
114 In this study, our first aim was to investigate to what extent allotriploidy may facilitate the
115 formation of COs near the cold recombining centromeric regions, by taking advantage of the
116 recently updated genome assembly of the *B. napus* cv. Darmor genome (Rousseau-Gueutin et al.
117 2020) that now contains the repeat rich (peri)centromeric regions. Additionally, it remained to be
118 deciphered if this modified recombination pattern may be kept or may revert back to a normal
119 strict meiotic behavior to prevent putative long-term genomic instabilities. To address these
120 questions, we firstly designed numerous markers specific to two pericentromeric regions.
121 Thereafter, we took advantage of the formation of some allotriploid (AAC) and allotetraploid
122 (AACC) individuals within the progeny of an AAC allotriploid hybrid, to investigate the impact
123 of the ploidy level in the following generation on homologous recombination. Overall, we
124 produced and genotyped a total of six segregating populations (different ploidy levels and
125 different generations). To compare the recombination frequency and distribution between these
126 hybrids, we performed comparative genetic mapping using the same anchored SNPs set
127 (including pericentromeric markers), and always validated them by HEI10 immunostaining on
128 Pollen Mother Cells (PMC) associated with GISH-like. From these analyses, we demonstrated

129 that (1) COs may occur as close as 375 kb from the centromere in an allotriploid compared to 4.5
130 Mb in an allotetraploid, (2) the modified recombination landscape can be maintained in
131 successive generations of allotriploidy, (3) a normal meiotic control is recovered in an
132 allotetraploid progeny of an allotriploid hybrid, (4) the recombination rate is increased within
133 hybrids of the second generation, whatever their ploidy levels. This novel knowledge is important
134 for both fundamental and applied research, as it increases our understanding on how allotriploidy
135 may play a major role in polyploid speciation, evolution and adaptation. In addition, the method
136 described here provides an efficient and easy way to naturally switch on and off a strict control of
137 recombination in polyploid crops, that can be used to greatly enhance their genetic diversity,
138 reduce linkage disequilibrium for some agronomic traits and favor the combination of favorable
139 alleles, or even facilitate the identification of candidate genes of interest.

140

141 **Results**

142 1. Meiotic behaviors, pollen viability and seed set within hybrids presenting varying ploidy
143 levels

144

145 As an initial step to analyzing the evolution over successive generations of the recombination
146 profile in *Brassica* hybrids harboring different ploidy levels, we investigated the meiotic behavior
147 at metaphase I of an allotetraploid ($A_nA_rC_nC_o$) and allotriploid ($A_nA_rC_n$) F1 hybrids presenting
148 the exact same A genotype, as well as their backcross progenies. To facilitate the reading, we
149 chose the following nomenclature to describe our hybrids, with first the ploidy level, then the
150 generation, and finally the maternal ploidy origin of each hybrid. Briefly, the F1 allotetraploid
151 and allotriploid hybrids are referred to 4x-F1 and 3x-F1, respectively. The descending
152 allotetraploid and allotriploid hybrids deriving from the backcross of the 3x-F1 were entitled 4x-
153 B1F1^{3x} and 3x-B1F1^{3x}, whereas the allotetraploid hybrid deriving from the backcross of the 4x-
154 F1 was referred to as 4x-B1F1^{4x}. More details on the genotypes and on the methods used to
155 create these hybrids is given in Figure 1.

156 For each hybrid, the meiotic behavior was firstly established using both classical aceto-carmine
157 staining and a GISH-like technique using the Bob014O06 BAC probe that specifically hybridizes
158 to all C chromosomes. The 3x-F1 and 4x-F1 hybrids showed the expected meiotic behavior, with

159 a majority of Pollen Mother Cells (PMC) with ten A bivalents plus nine C univalents for 3x-F1
160 and ten A bivalents plus nine C bivalents 4x-F1 (Table 1, Figure 2). We also assessed the pollen
161 viability and seed set of these hybrids and observed that the 3x-F1 presents a lower pollen
162 fertility compared to the 4x-F1 hybrid (69% and 97%, respectively, Table 1). Similarly, there is a
163 lower number of seeds per pollinated flower in the 3x-F1 compared to the 4x-F1 (2.3 vs 10.2,
164 respectively, Table 1). At the second generation, we chose to study two different 3x-B1F1^{3x}
165 hybrids carrying different heterozygous genomic regions in order to validate that whatever
166 the genetic structure of the hybrid we would observe the same meiotic recombination pattern. The
167 two selected 3x-B1F1^{3x} hybrids had an improved meiotic behavior compared to the 3x-F1, with
168 systematically ten A bivalents and nine C univalent. They presented a male fertility and seed set
169 similar to their parental mother plant 3x-F1 (Table 1, Figure 2). Concerning the 4x-B1F1^{3x} and
170 4x-B1F1^{4x}, they also both presented a similar meiotic behavior, pollen viability and seed set as
171 their mother 4x-F1 plant (Table 1, Figure 2).

172
173 In the following sections, we compared the recombination profile of these different hybrids by
174 performing genetic mapping using an identical set of polymorphic SNP markers for each
175 comparison. These results were thereafter complemented by the quantification of class I COs
176 frequency on the A sub-genome in PMC (male meiosis) at diakinesis, using HEI10
177 immunostaining coupled with GISH-like chromosome painting using the C-chromosome specific
178 BAC.

179
180 2. Allotriploidy increases recombination frequency and enables the formation of COs at the
181 vicinity of centromeres, notably via deeply reducing the strength of interference

182
183 Backcross populations of the 4x-F1 and 3x-F1 hybrids (always used as females) were previously
184 obtained and genotyped using *Brassica* Illumina Infinium SNP array (SGS-TraitGenetics GmbH,
185 Gatersleben, Germany). However, the recently improved *B. napus* cv. *Darmor* genome using the
186 third-generation sequencing technologies (Rousseau-Gueutin et al. 2020) enabled to assemble the
187 complex and repetitive-rich pericentromeric regions (Figure S1) and revealed that almost no
188 markers were in fact present in these regions. Indeed, in the previous study, the closest markers
189 surrounding the A01 and A02 centromeres were previously distant by 5 Mb and 7.6 Mb and thus

190 did not allow to identify the presence of COs in these regions. To circumvent this problem and
191 properly investigate the presence of COs near the centromere, we took advantage of the recent
192 improvements of both *B. napus* cv. Darmor and *B. rapa* cv. Chiifu genome assemblies (A parental
193 donors of our hybrids) to design many novel polymorphic KASPar markers in both A01 (81
194 markers) and A02 (25 markers) pericentromeric regions (Table S1). These two chromosomes
195 were chosen as that were polymorphic in most of the hybrids investigated in this study, including
196 most second-generation hybrids (3x-B1F1b^{3x}, 4x-B1F1^{3x}, 4x-B1F1^{4x}, see Figure 1).

197 Using the same set of polymorphic markers deriving from both the 15K array and these newly
198 designed KASPar markers (totalling 2274 SNPs), we generated genetic maps for both 3x-F1 and
199 4x-F1. As previously observed (Boideau et al. 2021), the 3x-F1 hybrid shows a significant 3.7-
200 fold increase of COs frequency compared to the 4x-F1 hybrid (Bonferroni corrected chi-squared
201 test (BcC test), $P < 2.2E-16$, Table S2).

202 When investigating more finely the pericentromeric regions, we found that the 4x-F1 hybrid had
203 no CO, whereas the 3x-F1 hybrid presented 36 COs in total (Table S2). Interestingly, these COs
204 can arise as close as 375 kb from the centromeric borders in the 3x-F1, while the nearest CO
205 detected for the 4x-F1 hybrid was localized 4.5 Mb from the centromeric border. We also
206 compared the strength of interference between these hybrids and observed that the level of
207 interference is significantly lower in the 3x-F1 compared to the 4x-F1 hybrid, with an estimated
208 Nu value of 1.847 and 9.588 respectively. Nevertheless, a slight interference was still detected in
209 the 3x-F1 hybrid according to the gamma model (testing if Nu was close to 1, $P < 0.001$).

210 The increased CO frequency in the 3x-F1 compared to 4x-F1 hybrids observed in female meiosis
211 using genetic mapping was thereafter validated using HEI10 immunostaining, labelling class I
212 COs on male meiocytes at diakinesis (24 in the 3x-F1 vs 18 in the 4x-F1 on average, Mann
213 Whitney Wilcoxon test (MWW test), $P = 2.05E-08$, Figures 3 and 4, Table S3).

214
215 3. The modified recombination profile observed in AAC allotriploids can be maintained by
216 performing successive generations at the allotriploid level with even a slight increase of
217 CO frequency

218
219 To determine if the modified recombination landscape observed in the 3x-F1 may be conserved
220 for successive generations at the allotriploid level, we searched for allotriploid plants in the

221 backcross progeny of the 3x-F1 using firstly flow cytometry. We identified 8 out of the 245
222 genotyped progenies that were potentially allotriploids. Their chromosome number were
223 thereafter validated at $2n=3x=29$ using molecular cytogenetics. It is important to note that as
224 these progenies were obtained via a backcross, on average only half of the A genome is expected
225 to be heterozygous. For the following analyses, we thus kept one 3x-B1F1b^{3x} hybrid, which was
226 heterozygote for the A01 and A02 pericentromere regions, allowing a comparison of these
227 regions in the successive generations. Comparative genetic mapping was only performed in the
228 common heterozygous regions between the 3x-B1F1b^{3x} and 3x-F1 hybrids (distributed in 18
229 regions of the ten A chromosomes, totaling 182.3 over the 346 Mb) using the same set of 1205
230 polymorphic SNP markers (Table 2, Figure 5), thus preventing biases when comparing their
231 recombination profiles. It revealed that the 3x-B1F1b^{3x} presents a similar recombination profile
232 with even a statistically significant 1.7-fold increase of recombination frequency compared to the
233 3x-F1 hybrid (BcC test, 3.82E-78). This significant increase was observed for non-
234 pericentromeric and pericentromeric regions (BcC test, $P = 1.36E-14$, 2.71E-65 respectively). It
235 was also validated in male meiosis using HEI10 immunostaining (1.18-fold increase, MWW test,
236 $P=1.27E-05$, Figure 3 and 4).

237 To further validate this increased recombination frequency in the 3x-B1F1b^{3x} compared to the 3x-
238 F1, similar experiments were performed on another 3x-B1F1a^{3x} plant. Comparative genetic maps
239 also showed a significant increase of recombination frequency (1.35 folds, BcC test, $P=1.92E-19$,
240 Table 1, Figure 5, Table S2) compared to the 3x-F1, while HEI10 immunostaining revealed a
241 slight but not significant increase of HEI10 foci (1.08-fold, MWW test, $P=0.98$, Figure 3 and 4,
242 Table S3). Therefore, the modified recombination profile observed in the 3x-F1 is maintained in
243 the 3x-B1F1 hybrid, with even a slight increase of the recombination frequency.

244
245 4. The deregulation of the recombination control provoked by allotriploidy can be switched
246 off and reverted back to normal in a descending allotetraploid individual

247
248 To decipher if the modified recombination landscape observed in the 3x-F1 hybrid may revert
249 back to a normal and strict meiotic control in the next generation, we firstly searched for an
250 allotetraploid individual in the backcross progeny of the 3x-F1 using both flow cytometry and
251 molecular cytogenetics. In total, we identified two potential allotetraploid progenies and we

252 chose one individual (referred as 4x-B1F1^{3x}, Figure 1) that was heterozygous for the A01 and
253 A02 pericentromeric regions. In this 4x-B1F1^{3x} plant, we could identify 17 polymorphic regions,
254 totaling as expected about half of the A genome. We performed comparative genetic mapping
255 between the 4x-B1F1^{3x} and 3x-F1 (Figure 5, Table 2) and observed a significant 2.6-fold decrease
256 of the recombination frequency in the 4x-B1F1^{3x} compared to the 3x-F1 hybrid (BcC test, P =
257 2.45E-19, Table 1, Table S2). A significant decrease of class I COs was also observed in male
258 meiosis using HEI10 immunostaining (1.24-fold, MWW test, P = 5.92E-05, Figure 3 and 4, Table
259 S3).

260 Interestingly, using both comparative genetic mapping or HEI10 immunostaining, the decrease of
261 the recombination frequency observed in the 4x-B1F1^{3x} was smaller than expected, compared to
262 the observed 3.7-fold observed between the 4x-F1 and the 3x-F1. The smaller decrease of the
263 recombination frequency in the 4x-B1F1^{3x} can either be due to a residual effect from the
264 allotriploid step or to its backcross origin, with only half of the genome that contains
265 heterozygous regions juxtaposed to homozygous regions. To test these hypotheses, we compared
266 the recombination frequency between a 4x-B1F1^{4x} and a 4x-F1 hybrid using both genetic
267 mapping and HEI10 immunostaining (Table 2, Figure 4). We observed an increased
268 recombination frequency in the 4x-B1F1^{4x} compared to the 4x-F1, as previously observed for the
269 allotriploid lineage. We also compared the recombination frequency between a 4x-B1F1^{3x} and 4x-
270 B1F1^{4x} using the same set of markers, and surprisingly observed slightly more recombination in
271 the 4x-B1F1^{4x} compared to the 4x-B1F1^{3x} (BcC test, P = 0.026). However, this difference was
272 only due to one region on the chromosome A07 (BcC test, P = 0.085). Altogether, these results
273 highlight an absence of residual effect from the allotriploid step and suggests that the increased
274 recombination frequency observed in the second generation is a result of the backcrossing.

275

276 **Discussion**

277 In this study, we further investigated the modified recombination pattern discovered in *Brassica*
278 allotriploids. First, we determined unambiguously that the intriguing recombination profile
279 observed in allotriploids enables the formation of numerous COs in the normally low
280 recombining pericentromeric regions. Secondly, we identified individuals of different ploidy
281 levels (either allotriploid or allotetraploid) at the following generation and determined that it was
282 either possible to naturally maintain this deregulation of recombination or to revert it back to a

283 normal strict meiotic control. Finally, we discuss the potential origins of this meiotic deregulation
284 and the important role that allotriploidy may play in polyploid diversification and establishment.

285 *Allotriploidy massively increases the CO formation in the normally low recombining*
286 *pericentromeric regions*

287 In spite of the hypothesis that the absence of COs in centromeric regions may be related to the
288 key role of this chromosomal region in the proper segregation of chromosomes (McKinley and
289 Cheeseman, 2016), we demonstrated that they occur in natural allotriploid hybrids at a high
290 frequency in pericentromeric regions. Due to their key cellular function, the centromeric regions,
291 which are composed of megabase of satellite repeat arrays (Naish et al. 2021), are lacking COs
292 (Fernandes et al. 2024). Even large regions (several Mb) surrounding the centromeres present a
293 very low recombination rate, as recently exemplified in Arabidopsis (Fernandes et al. 2024) or
294 also in crops, such as barley (Dreissig et al. 2020) and wheat (Raz et al. 2021). Here, we took
295 advantage of the recent improvements of *B. napus* cv. Darmor (Rousseau-Gueutin et al. 2020)
296 and *B. rapa* cv. Chiifu (Zhang et al. 2018) genome assemblies, which now includes the
297 pericentromeres, to determine if allotriploidy facilitates the formation of COs in these latter
298 regions. Indeed, our previous study (Pele et al. 2017) that used the first *B. rapa* genome assembly
299 (Wang et al. 2011) did in fact not contain any pericentromeric marker from these regions,
300 preventing us to truly test this hypothesis. To that purpose, we designed numerous novel KASPar
301 markers specific to the pericentromeric regions of chromosomes A01 and A02 spanning 8.2 Mb
302 and 7.1 Mb, respectively, and that were heterozygous in most of our investigated hybrids (five
303 out of six). This marker enrichment enabled us to demonstrate that numerous COs occur in these
304 normally cold pericentromeres in allotriploids as 36 out of 131 individuals had a CO compared to
305 none in an allotetraploid population of 172 individuals. Additionally, COs may occur as close to
306 375 kb from the centromere border in allotriploids compared to 4.5 Mb in allotetraploids. In
307 plants, the quasi absence of COs in the pericentromeric regions correlate with the presence of
308 high DNA methylation and an enrichment for heterochromatic histone marks, such as H3K9me2
309 (Fernandes et al. 2024). So far, the only other examples where the CO frequency increased in
310 these pericentromeric low recombining regions was observed after performing the K.O. of the
311 *CMT3* gene in Arabidopsis, which reduced both CHG DNA methylation and H3K9me2
312 (Underwood et al. 2018, Fernandes et al. 2024). However, this deregulation was at a much

313 smaller magnitude compared to our allotriploid model. In addition, the use of the Crispr-Cas9
314 technology may be longer and more difficult as each gene is often present in several copies in
315 most crops, as most of them are (paleo)polyploids (Facon et al. 2023). The natural method we
316 present here and that plays with the ploidy level will be far more efficient for generating genetic
317 diversity in these pericentromeric regions. This is crucial as pericentromeric regions are far from
318 being deprived of expressed genes, including genes of interests (Boideau et al. 2021, Rousseau-
319 Gueutin et al. 2020, Fernandes et al. 2024). For example, the *B. napus* cv. Darmor A01 and A02
320 pericentromeric regions contain 662 and 505 genes, representing 15.64 and 11.31% of the genes
321 present on the A01 and A02 chromosomes, respectively. Additionally, some of these
322 pericentromeric genes can be associated to genes involved in agronomic traits of interests, as 28
323 and 25 Resistant Gene Analogs were identified in these A01 and A02 pericentromeric regions,
324 according to Rousseau-Gueutin et al. (2020). Recently, the particular interest of using Brassica
325 allotriploidy to decrease the size of a QTLs present in pericentromeric regions was highlighted by
326 a modelling study (Tourette al. 2021) and exemplified for a pericentromeric QTL conferring
327 blackleg resistance (Boideau et al. 2021).

328 *A natural method enabling to switch on and off the strict meiosis regulation*

329 In *Brassica*, allotriploidy was shown to deeply modify the recombination landscape (Pelé et al.
330 2017, Boideau et al. 2021). However, it remained to be determined whether this modification
331 may be maintained for successive generations to take advantage of this meiotic deregulation or
332 revert back to normal to prevent potential longer-term genomic instabilities (Vincenten et al.,
333 2015). To test this hypothesis, we identified an AAC and AACC progenies from the first
334 allotriploid hybrid. We were able to show that the maintenance of an allotriploid level at the
335 second generation allows to keep this modified recombination pattern, including the presence of
336 CO in the normally cold recombining pericentromeric regions. On the contrary, we demonstrated
337 that recovering an allotetraploid individual can immediately switch off this deregulation. This
338 descending allotetraploid individual recovered a normal meiotic behavior and a seed set similar to
339 most cultivated allotetraploid *B. napus* varieties (Siles et al. 2021). The observation of the
340 presence of a modified recombination pattern only in allotriploid but never in allotetraploid
341 hybrids (whatever the generation) strongly indicates that interploidy (i.e. presence of one genome
342 in single copy, where all its chromosomes remain as univalent during meiosis) is at the origin of

343 this modification of the recombination control. Recently, the identification of a similar meiotic
344 deregulation a wheat allopolyploid ($2n=5x=35$, *AABB*D; Yang et al. 2022) strongly comforts this
345 hypothesis and suggests that this phenomenon may be common to many polyploid flowering
346 plants. Given the important number of polyploid crops, and that many of them present an eroded
347 genetic diversity, this modification of the recombination control via interploidy could deeply
348 increase and shuffle their genetic diversity. Indeed, many of these polyploid crops can be crossed
349 to their parental progenitor of a smaller ploidy level and give rise to a still fertile interploid
350 hybrid, as exemplified in wheat (Vardi and Zohary, 1967), coffee (Krug and Mendes, 1940),
351 strawberries (Yarnell et al. 1931), tomato (Rick et al. 1988) or tobacco (East et al. 1933).

352 Altogether, the easy recovery of an allotetraploid *B. napus* individual in the progeny of an
353 allotriploid hybrid, associated with a stable meiosis and an improved seed set, is a proof of
354 concept that the allotriploid pathway is of high relevance (i) to speed up and reduce the costs of
355 some breeding programs by reducing the size of segregating populations and number of
356 individuals to be genotyped, (ii) to reduce the size of *B. rapa* introgressed regions of interests
357 (preventing the parallel introgression of deleterious alleles), (iii) and lastly to reduce the linkage
358 disequilibrium observed within *B. napus*.

359 *Origin of the recombination modification*

360 It is yet to be deciphered what factors may be at the origin of this intriguing modification of the
361 recombination control in interploid species. One factor that may be involved in this phenomenon
362 is the delay of meiosis progression, especially in prophase of such interploidy individual. Indeed,
363 it has been observed that univalents move more slowly than paired chromosomes, potentially
364 increasing the duration of meiosis (Carlton et al. 2006, Cortes et al. 2015) and therefore
365 potentially increasing the formation of COs. However, this cannot be the only factor as there is
366 not a linear increase of the homologous recombination rate with the number of C chromosomes in
367 addition (Suay et al. 2014). Indeed, it has been observed that the increased homologous
368 recombination frequency observed in such individual was mainly explained by the addition of
369 C09, and also to a lesser extent by the C06 chromosomes (Suay et al. 2014), indicating a genetic
370 control of this phenomenon. This observation might be related to the presence on such
371 chromosomes of some dosage sensitive meiotic genes, as demonstrated for *HEI10* (Ziolkowski et
372 al. 2017) and *ASY1* (Lambing et al. 2020) in *A. thaliana*, *ASY3* in *B. napus* (Chu et al. 2024) or

373 *FIGL1* in *Z. mays* (Zhang et al. 2023), associated with a limited number of homologous
374 chromosomes that can pair. A third factor that may be participating in this phenomenon relates to
375 epigenetic modifications. In the monkeyflower *Mimulus*, it has notably been showed that
376 allotriploidy was at the origin of DNA demethylation and that a partial remethylation occurred
377 when recovering an allohexaploid (Edger et al. 2017). As observed from the K.O. of some
378 epigenetic genes in *Arabidopsis*, the decrease of DNA methylation but also of some repressive
379 histone marks, such as H3K9me2, may modify COs distribution (Melamed-Bessudo and Levy
380 2012, Yelina et al. 2012, Underwood et al. 2018, Fernandes et al. 2024). The potential link that
381 may exist between DNA methylation or chromatin compaction remains to be investigated in
382 meiotic cells of such allotriploid hybrids.

383 The comparison of the first- and second-generation hybrids (from the same ploidy level) revealed
384 here the presence of a slight increase of CO frequency in the second-generation, which may be
385 associated to the juxtaposition effect identified in *Arabidopsis* (Ziolkowski et al. 2015). In this
386 latter species, it has been observed a slight increase of 1.35-fold in the heterozygous region that
387 was juxtaposed to a homozygous region (Ziolkowski et al. 2015). The juxtaposition effect
388 corresponds to a MSH2-dependant local redistribution of Class I COs towards polymorphic
389 heterozygous regions to the detriment of the juxtaposed homozygous regions, in *A. thaliana*
390 (Blackwell et al. 2020). Similarly, a slight increase of recombination in BC2 compared to BC1
391 hybrids was observed in *B. oleracea* (1.66-fold: Kearsey et al. 1996). Therefore, this effect may
392 be general at least to Brassicaceae and be considered in some breeding programs.

393 *Putative role of an allotriploid step in the speciation success of a newly formed polyploid*

394 Allopolyploid species may arise by numerous routes. They may form via the merging of two
395 divergent diploid genomes through the formation of an allodiploid (i.e. homoploid bridge),
396 allotriploid (i.e. unilateral pathway) or allotetraploid (i.e. bilateral pathway) hybrids (Tayale and
397 Parisod, 2013, Pelé et al. 2018). In several polyploid species, only a few allopolyploidisation
398 events were at their origin. To increase its population size, a new polyploid may produce
399 progenies through self-fertilization or via crossing with one of its parental species. That latter
400 route will form allotriploid individuals presenting this deregulated recombination pattern.
401 Thereafter, the selfing of this allotriploid and/or its backcrossing with an allotetraploid individual
402 will thus give rise to more genetically diversified allotetraploid individuals. A recent study from

403 Cao et al. (2023) revealed that within three generations of self-fertilization, allotriploids mainly
404 developed near complete allotetraploid individuals via gradually increasing the chromosome
405 number and fertility. Indeed, natural selection strongly acts and favors the genomically stable
406 allotetraploid progenies over interploid or aneuploid individuals. Nevertheless, during these few
407 intermediate generations of aneuploidy, it is likely that these individuals also presented a
408 modified recombination pattern (but at a lesser extent), as previously observed in *Brassica* (Suay
409 et al. 2014). Thus, allotriploidy, with aneuploidy as intermediate, can play a major role in
410 polyploid genetic diversification and potential adaptation, facilitating their potential
411 establishment and speciation success. These results further support the importance of
412 allotriploidy as a bridge in polyploid speciation.

413

414 **Material and Methods**

415 - Plant material

416 The plant material analyzed in this study is described in Figure 1. To distinguish the different
417 genomes, we used as nomenclature A_r and A_n for the A genome of *B. rapa* and *B. napus*,
418 respectively, whereas we used C_o and C_n for the C genome of *B. oleracea* and *B. napus*,
419 respectively. The term “Rec” as index indicates that recombination occurred on the genome
420 concerned. To produce an allotriploid AAC and allotetraploid AACC hybrids presenting a
421 genetically identical A genome sequence enabling an unbiased comparison of their recombination
422 profile, we used the following strategy. To produce the allotetraploid hybrid (4x-F1), we firstly
423 created a resynthesized oilseed rape, which was obtained by crossing the pure inbred line *B. rapa*
424 cv. Chiifu (A_rA_r , $2n=2x=20$) with the doubled haploid *B. oleracea* cv. HDEM (C_oC_o , $2n=2x=18$;
425 used as male) and then by performing embryo rescue on the obtained amphihaploid (A_rC_o ,
426 $2n=19$) as described earlier (Jahier et al. 1992). This hybrid spontaneously doubled its genomes
427 and gave rise to the resynthesized allotetraploid $A_rA_rC_oC_o$ ($2n=4x=38$), hereafter referred as
428 ChEM. This latter plant was crossed with *B. napus* cv. Darmor ($A_nA_nC_nC_n$) as female, and the
429 $A_nA_rC_nC_o$ F1 hybrid referred as 4x-F1 gave rise to 172 B1F1 plants after backcrossing with
430 recurrent parent *B. napus* cv. Darmor as male (Boideau et al. 2021). One of these B1F1 plants
431 with ~50% of A and C genome at the heterozygous stage was kept ($A_{Rec}A_nC_{Rec}C_n$, $2n=4x=38$,
432 referred as 4x-B1F1^{4x}) to produce a B2F1 segregating population (172 plants) by backcrossing it
433 with *B. napus* cv. Darmor as male (Figure 1).

434 For the allotriploid pathway, an allotriploid F1 hybrid ($A_nA_rC_n$, $2n=3x=29$, referred as 3x-F1) was
435 obtained by crossing the allotetraploid *B. napus* cv. Darmor $A_nA_nC_nC_n$ ($2n=4x=38$) and *B. rapa*
436 cv. Chiifu (A_rA_r , $2n=2x=20$) as male. For the production of its B1F1 progeny, the hybrid was
437 crossed with *B. napus* cv. Darmor as male. We selected 131 plants to generate the mapping
438 population of the 3x-F1 hybrid (Boideau et al. 2021). Within this latter B1F1 population, we
439 selected two AAC allotriploid hybrid progenies ($A_{Rec}A_nC_n$, $2n=3x=29$, hereafter referred to as 3x-
440 B1F1a^{3x} and 3x-B1F1b^{3x}) and one allotetraploid hybrid progenies ($A_{Rec}A_nC_nC_n$, $2n=4x=38$,
441 referred as 4x-B1F1^{3x}) based on their meiotic behavior and on the common polymorphic regions.
442 Then, these three hybrids were backcrossed to *B. napus* cv. Darmor as male, giving rise to three
443 mapping populations of 130, 130 and 172 plants, respectively (Figure 1). All parental accessions
444 were provided by the Biological Resource Center BrACySol (INRAe, Ploudaniel, France).

445
446 - DNA extraction and genotyping
447 Genomic DNA was extracted from lyophilized young leaves with the sbeadex maxi plant kit
448 (LGC Genomics, Teddington Middlesex, UK) on the oKtopure robot at the GENTYANE
449 platform (INRAe, Clermont-Ferrand, France). Genotyping data were obtained using the *Brassica*
450 15K and 19K Illumina Infinium SNP array (SGS TraitGenetics GmbH, Gatersleben, Germany).

451
452 To assess recombination within the pericentromeric region of A01 and A02 chromosomes that
453 contained a very low number of polymorphic SNPs between our parental lines, we then
454 developed an additional set of markers to specifically densify these pericentromeric regions. The
455 improved assembly of pericentromeric regions between *B. napus* cv. Darmor v10 (Rousseau-
456 Gueutin et al. 2020) and v5 genome assemblies (Chalhoub et al. 2014) can be visualized in
457 Figure S1, which was obtained by comparing their assemblies using SyRI (Goel et al. 2019) with
458 default parameters.

459 To design A01 and A02 pericentromeric markers, we firstly took advantage of the presence of
460 polymorphic markers between our parental lines using data from the Brassica 60K Illumina
461 Infinium SNP array (Clarke et al. 2016). This enabled us to identify 48 polymorph markers that
462 were absent from the 15K and 19K Brassica Illumina Infinium arrays and for which we
463 developed KASPar markers using their context sequences. We also designed 39 additional
464 KASPar markers closer to the A01 and A02 centromeres by taking advantage of the whole

465 genome assembly of the parental lines (Zhang et al. 2018, Rousseau-Gueutin et al. 2020). To
466 design these new SNP within our intervals of interest, we firstly retrieved the genes present in
467 single copy in each *B. napus* cv. Darmor-bzh v10 subgenome (Rousseau-Gueutin et al. 2020) and
468 in *B. rapa* cv. Chiifu v3 (Zhang et al. 2018), preventing the putative design of markers
469 amplifying on different paralogous regions. The orthologous copy of these genes in *B. oleracea*
470 cv. HDEM were also retrieved using BlastP. For each of these genes, we performed an alignment
471 of the different copies (*B. rapa*, *B. napus* copy A and copy C, *B. oleracea*) and used an in-house
472 python script to specifically detect polymorphism between the A chromosomes of *B. napus* cv.
473 Darmor and *B. rapa* cv. Chiifu. Overall, genotyping data were obtained for this novel set of 87
474 SNP markers (specific to the A01 and A02 pericentromeric regions, details for these markers are
475 given in Table S1) and revealed by BiomarkTM HD system (Fluidigm technology) and KASParTM
476 chemistry at the GENTYANE platform (INRAE, Clermont-Ferrand, France). The raw
477 genotyping data deriving from the Brassica Illumina Infinium arrays or from the KASPar
478 technology were analyzed using either the GenomeStudio v.2011.1 (Illumina Inc., San Diego,
479 CA, USA) or the Fluidigm SNP Genotyping Analysis v4.1.2 softwares (Wang et al. 2009). In
480 both cases, the raw genotyping data were processed with the auto-clustering option and validated
481 manually. The polymorphic SNPs between the parental genotypes were selected for the
482 establishment of genetic maps. SNPs showing more than 20% of missing data and plants showing
483 more than 25% of missing data were removed for the downstream analyses. Potential double
484 crossovers supported by only one genetic marker and with a physical distance between these two
485 events below 500 kb was corrected as missing data, as described in Rowan et al. (2019). To
486 prevent the overestimation of recombination in the low recombining pericentromeric regions,
487 plants showing more than one CO in the pericentromeric region of A01 and A02 were removed.
488 Finally, to determine the physical position of the different markers, the context sequences of each
489 SNP marker were physically localized on the reference genome *B. napus* cv. Darmor-bzh v10
490 (Rousseau-Gueutin et al. 2020) by using BlastN (ver. 2.9.0, min. e-value 1×10^{-20} , Altschul et
491 al. 1990) and by keeping the best blast hit obtained for a given subgenome (minimum percentage
492 of alignment and identity of 80%).

493

494 - Genetic maps

495 The first genetic maps were established separately for each population using the CarthaGene
496 software (v. 1.2.3, De Givry et al. 2005). Establishment of linkage groups and SNP ordering were
497 determined using a logarithm of odds score (LOD) threshold of 4.0 and a threshold
498 recombination frequency of 0.3, as previously described (Pelé et al. 2017). After these few
499 corrections, the final genetic maps were created using the Kosambi function to evaluate the
500 genetic distances in centimorgans (cM) between linked SNP markers (Kosambi, 1943).
501 Genotyping data used are available in Table S1. The genetic landscapes were illustrated using
502 Circos v0.69-9 (Krzywinski et al. 2009).

503
504 The pericentromeric and centromeric borders were retrieved from Boideau et al. (2022) and were
505 based on gene density and centromeric-specific repeats, respectively. Precisely, pericentromeric
506 regions were defined as regions surrounding the centromere and characterized by a gene density
507 below the chromosome average. Hereafter, a pericentromeric interval refers to the interval
508 between the pericentromeric borders, corresponding to both the centromeric and pericentromeric
509 regions.

510
511 - Interference
512 The interference parameters using the Gamma model were determined using the software CODA
513 with the default parameters (Gauthier et al. 2011). Confidence intervals and statistical tests were
514 not based on Fisher's gaussian approximation as proposed in the graphical user interface of
515 CODA but were performed based on 1000 resimulations using the command-line interface *via*
516 custom perl and R scripts.

517
518 - Flow cytometry and cytogenetic studies
519 Chromosome numbers of the allotriploid progenies were assessed in leaves by flow cytometry as
520 described in Leflon et al. (2006). Pollen viability was assessed from three independent flowers,
521 using acetocarmine staining, as described in Jahier et al. (1992). For the establishment of meiotic
522 behavior, samples of young floral buds were fixed in Carnoy's II solution
523 (alcohol:chloroform:acetic acid, 6:3:1) for 24 h at room temperature and stored until use in 50%
524 ethanol at 4 °C. Anthers were then squashed and stained with a drop of 1% acetocarmine

525 solution. Chromosome pairing was assessed per plant from 20 Pollen Mother Cells (PMCs) at
526 metaphase I.

527 a) Meiotic proteins immunolocalization

528 The immunolabelling of HEI10 was carried out on meiotic chromosome spread prepared as
529 described in Chelysheva et al. (2013) with minor modifications. Briefly, the chromosome
530 preparations were incubated in Rnase A (100ng/μL) and pepsin (0.05%) in 10 mmol HCL,
531 dehydrated in an ethanol series (70%, 90% and 100%) and air-dried. The anti-HEI10 antibody
532 was used at a dilution of 1/100^o in 1X PBS-T-BSA. The slides were incubated overnight at 4°C.

533 After three rinses in 1X PBS-T, slides were incubated for 1h at room temperature with a labeled
534 secondary antibody (labeled goat anti-rabbit IgG Alexa fluor 488-Invitrogen (ref. A-11008,
535 Invitrogen) diluted 1/200 in 1X PBS-T-BSA. After three rinses in 1X PBS-T, the slides were
536 mounted in Vectashield (Vector Laboratories) containing 2.5μg/mL of 4',6-diamidino-2-
537 phenylindole (DAPI). Fluorescence images were captured using an ORCA-Flash4 (Hamamatsu,
538 Japan) on an Axioplan 2 microscope (Zeiss, Oberkochen, Germany) and analyzed using Zen PRO
539 software (version 2, Carl Zeiss, Germany).

540

541 b) GISH-like at meiosis using a genome specific BAC clone

542 For observation of HEI10 foci only on A paired chromosomes, the BAC clone BoB014O06 from
543 *B. oleracea* (Howell et al. 2002) was used as a probe for the C genome on the same cells. This
544 GISH-like BAC hybridized specifically to regions on every C-genome chromosome in *B. napus*
545 (Książczyk et al, 2011). The BoB014O06 probe was labelled by random priming with biotin-14-
546 dUTP (Invitrogen, Life Technologies). The hybridization mixture, consisting of 50% deionized
547 formamide, 10% dextran sulfate, 2X SSC, 1% SDS and labelled probes (200ng per slide), was
548 denatured at 92°C for 6 min and transferred to ice. The denatured probe was placed on the
549 chromosome preparation and *in situ* hybridization was carried out overnight in a moist chamber
550 at 37°C. After hybridization, slides were washed for 5 min in 50% formamide in 2X SSC at
551 42°C, followed by two washes in 4X SSC-Tween. Biotinylated probe was immunodetected by
552 Texas Red avidin DCS (Vector Laboratories) and the signal was amplified with biotinylated anti-
553 avidin D (Vector Laboratories). The chromosomes were mounted and counterstained in
554 Vectashield (Vector Laboratories) containing 2.5μg/mL 4',6-diamidino-2-phenylindole (DAPI).

555 Fluorescence images were captured using an ORCA-Flash4 (Hamamatsu, Japan) on an Axioplan
556 2 microscope (Zeiss, Oberkochen, Germany) and analyzed using Zen PRO software (version 2,
557 Carl Zeiss, Germany).

558 - Statistical analyses

559 Comparison of the crossover rates between progenies was assessed for every interval between
560 consecutive SNP markers using a 2-by-2 chi-squared analysis considering a significance
561 threshold of 5%. Additionally, these comparisons were also performed for a given heterozygous
562 region, at the chromosome and at the genome scales using 2-by-2 chi-squared tests. For these
563 tests, a conservative Bonferroni-corrected threshold of 5% was applied, using either the number
564 of regions, the number of chromosomes or the number of intervals between adjacent SNP
565 markers per A chromosome, or for the whole A subgenome (as described in Pelé et al. 2017 and
566 Boideau et al. 2021). Statistical comparisons of the interference strength were assessed using the
567 software CODA (Gauthier et al. 2011). Statistical differences for the number of HEI10 foci
568 between the different hybrids were assessed using the Mann Whitney Wilcoxon statistical test
569 and considering a significance threshold of 5%, with a conservative Bonferroni-corrected
570 threshold of 5%. All statistical analyses were performed using RStudio (version 3.6.1, R Core
571 Team, 2021).

572 **Acknowledgments**

573 We thank the Genetic Resource Center BrACySol (INRAe, Ploudaniel, France,
574 https://www6.rennes.inrae.fr/igepp_eng/About-IGEPP/Platforms/BrACySol) for providing seeds
575 of the parental lines. We would like to thank all the staff who took care of our plant material
576 (especially L. Charlon, P. Rolland, J-P. Constantin, J. M. Lucas and F. Letertre). We also thank
577 the UMR 1905 GENTYANE Platform (especially C. Poncet, INRAe, Clermont-Ferrand, France,
578 <http://gentyane.clermont.inra.fr>) for performing DNA extractions and KASPar genotyping. We
579 thank SGS TraitGenetics (especially M. Ganal) for generating the genotyping data from the 15K
580 and 19K Brassica Illumina Infinium array (Gatersleben, Germany,
581 <http://www.traitgenetics.com/>). We warmly thank the plant molecular cytogenetic platform
582 (INRAe, Biogenouest, Le Rheu, France, [https://www6.rennes.inrae.fr/igepp_eng/About-](https://www6.rennes.inrae.fr/igepp_eng/About-IGEPP/Platforms/Molecular-Cytogenetics-Platform-PCMV)
583 [IGEPP/Platforms/Molecular-Cytogenetics-Platform-PCMV](https://www6.rennes.inrae.fr/igepp_eng/About-IGEPP/Platforms/Molecular-Cytogenetics-Platform-PCMV)) for helping and participating in
584 the cytogenetic experiments of this study. We thank Mathilde Grelon for providing the HEI10

585 antibodies, sharing protocols and productive discussions. We thank Eric Jenczewski for his
586 pertinent remarks to improve the project. We are thankful to Davy Soleilhet for important insight
587 into image analysis with the Zeiss Zen software. We thank the GOGEP team and GenOuest
588 bioinformatic platform (Rennes, France, <https://www.genouest.org/>), especially F. Legeai, S.
589 Robin, M. Boudet and A. Bretaudeau.

590 **Contributions**

591 FB, A-MC and MR-G designed the study. FB performed the genetic maps and statistical analyses.
592 LM contributed to the automatization of the genetic map establishment. AB and VH performed
593 the HEI10 experiments. AB, VH, GT, OC and FB analyzed the HEI10 images. GT and VH
594 performed and analyzed the MI BAC FISH meiotic behavior. ML-T took care of the DNA
595 samples. ML-T, GD, CF and FB analyzed the genotyping data. FE performed the classical
596 meiotic behavior. MG generated and took care of the plant material. JB designed the additional
597 pericentromeric SNP. JM generated the Circos representations. MF and OM analyzed the
598 interference. FB, MR-G and AM-C wrote the manuscript. All authors approved the final version
599 of the manuscript.

600 **Data availability**

601 All data analyzed in this study are provided as supplementary material.

602 **Funding**

603 This work was made possible by the financial support of the ANR ‘Stirrer’ (ANR-19-CE20-001
604 awarded to MR-G). This project also received funding from INRAE ‘Biology and Plant
605 Breeding’ department to perform part of the experiments presented here (projects ‘Recipe’ and
606 ‘Recoptic’ awarded to MR-G and A-MC respectively), as well as for part of FB’s PhD salary. We
607 also thank the ‘Region Bretagne’ that financed the second half of FB’s PhD salary (project
608 ‘Diverse’). GQE and IPS2 benefit from the support of Saclay Plant Sciences-SPS (ANR-17-
609 EUR-0007).

610

611 **References**

612 **Altschul, S.F., Gish, W., Miller, W., Myers, E.W., and Lipman, D.J.** (1990). Basic local
613 alignment search tool. *Journal of Molecular Biology* **215**: 403–410.

- 614 **Blackwell, A.R., Dluzewska, J., Szymanska-Lejman, M., Desjardins, S., Tock, A.J., Kbir,**
615 **N., Lambing, C., Lawrence, E.J., Bieluszewski, T., Rowan, B., Higgins, J.D.,**
616 **Ziolkowski, P.A., and Henderson, I.R.** (2020). MSH2 shapes the meiotic crossover
617 landscape in relation to interhomolog polymorphism in Arabidopsis. *The EMBO Journal* **39**:
618 e104858.
- 619 **Boideau, F., Pelé, A., Tanguy, C., Trotoux, G., Eber, F., Maillet, L., Gilet, M., Lodé-**
620 **Taburel, M., Huteau, V., Morice, J., Coriton, O., Falentin, C., Delourme, R.,**
621 **Rousseau-Gueutin, M., and Chèvre, A.M.** (2021). A Modified Meiotic Recombination
622 in *Brassica napus* Largely Improves Its Breeding Efficiency. *Biology* **10**.
- 623 **Boideau, F., Richard, G., Coriton, O., Huteau, V., Belser, C., Deniot, G., Eber, F., Falentin,**
624 **C., Ferreira de Carvalho, J., Gilet, M., Lodé-Taburel, M., Maillet, L., Morice, J.,**
625 **Trotoux, G., Aury, J.M., Chèvre, A.M., and Rousseau-Gueutin, M.** (2022). Epigenomic
626 and structural events preclude recombination in *Brassica napus*. *New Phytologist* **234**: 545–
627 559.
- 628 **Brubaker, C.L., Paterson, A.H., and Wendel, J.F.** (1999). Comparative genetic mapping of
629 allotetraploid cotton and its diploid progenitors. *Genome* **42**: 184–203.
- 630 **Cai, C., Pelé, A., Bucher, J., Finkers, R., and Bonnema, G.** (2023). Fine mapping of meiotic
631 crossovers in *Brassica oleracea* reveals patterns and variations depending on direction and
632 combination of crosses. *Plant J.* **113**: 1192–1210.
- 633 **Cao, Y., Zhao, K., Xu, J., Wu, L., Hao, F., Sun, M., Dong, J., Chao, G., Zhang, H., Gong, X.,**
634 **Chen, Y., Chen, C., Qian, W., Pires, J. C., Edger, P. P., and Xiong, Z.** (2023). Genome
635 balance and dosage effect drive allopolyploid formation in *Brassica*. *Proceedings of the*
636 *National Academy of Sciences of the United States of America*, *120*(14), e2217672120.
- 637 **Capilla-Pérez, L., Durand, S., Hurel, A., Lian, Q., Chambon, A., Taochy, C., Solier, V.,**
638 **Grelon, M., and Mercier, R.** (2021). The synaptonemal complex imposes crossover
639 interference and heterochiasmy in Arabidopsis. *Proceedings of the National Academy of*
640 *Sciences* **118**: e2023613118.
- 641 **Capilla-Pérez L., Solier, V., Gilbault, E., Lian, Q., Goel, M., Huettel, B., Keurentjes, J. J.**
642 **B., Loudet, O., and Mercier, R.** (2024). Enhanced recombination empowers the detection
643 and mapping of Quantitative Trait Loci. *Research Square* [[https://doi.org/10.21203/rs.3.rs-](https://doi.org/10.21203/rs.3.rs-3837166/v1)
644 [3837166/v1](https://doi.org/10.21203/rs.3.rs-3837166/v1)]
- 645 **Carlton, P.M., Farruggio, A.P., and Dernburg, A.F.** (2006). A Link between Meiotic Prophase
646 Progression and Crossover Control. *PLOS Genetics* **2**: e12.
- 647 **Chalhoub, B., Denoeud, F., Liu, S., Parkin, I. A., Tang, H., Wang, X., Chiquet, J., Belcram,**
648 **H., Tong, C., Samans, B., Corr ea, M., Da Silva, C., Just, J., Falentin, C., Koh, C. S.,**
649 **Le Clainche, I., Bernard, M., Bento, P., Noel, B., Labadie, K., ... Wincker, P.** (2014).
650 Plant genetics. Early allopolyploid evolution in the post-Neolithic *Brassica napus* oilseed
651 genome. *Science*, *345*(6199), 950–953.

- 652 **Chelysheva, L. A., Grandont, L., and Grelon, M.** (2013). Immunolocalization of meiotic
653 proteins in Brassicaceae: method 1. *Methods in molecular biology (Clifton, N.J.)*, 990, 93–
654 101.
- 655 **Choi, K., Zhao, X., Kelly, K.A., Venn, O., Higgins, J.D., Yelina, N.E., Hardcastle, T.J.,**
656 **Ziolkowski, P.A., Copenhaver, G.P., Franklin, F.C.H., McVean, G., and Henderson,**
657 **I.R.** (2013). Arabidopsis meiotic crossover hot spots overlap with H2A.Z nucleosomes at
658 gene promoters. *Nature Genetics* **45**: 1327–1336.
- 659 **Choi, K. and Henderson, I.R.** (2015). Meiotic recombination hotspots - A comparative view.
660 *Plant Journal* **83**: 52–61.
- 661 **Chu, L., Zhuang, J., Geng, M., Zhang, Y., Zhang, C., Schnittger, A., Yi, B., and Yang, C.**
662 (2024). ASY3 has dosage-dependent diverse effects on meiotic crossover formation.
663 bioRxiv: 2024.01.09.574930.
- 664 **Clarke, W.E., Higgins, E.E., Plieske, J., Wieseke, R., Sidebottom, C., Khedikar, Y., Batley,**
665 **J., Edwards, D., Meng, J., Li, R., Lawley, C.T., Pauquet, J., Laga, B., Cheung, W.,**
666 **Iniguez-Luy, F., Dyrszka, E., Rae, S., Stich, B., Snowdon, R.J., Sharpe, A.G., Ganal,**
667 **M.W., and Parkin, I.A.** (2016). A high-density SNP genotyping array for *Brassica napus*
668 and its ancestral diploid species based on optimised selection of single-locus markers in the
669 allotetraploid genome. *Theoretical and Applied Genetics* **129**: 1887–1899.
- 670 **Coop, G. and Przeworski, M.** (2022). Lottery, luck, or legacy. A review of “The Genetic
671 Lottery: Why DNA matters for social equality.” *Evolution* **76**: 846–853.
- 672 **Cortes, D.B., McNally, K.L., Mains, P.E., and McNally, F.J.** (2015). The asymmetry of female
673 meiosis reduces the frequency of inheritance of unpaired chromosomes. *eLife* **4**: e06056.
- 674 **Crismani, W., Girard, C., Froger, N., Pradillo, M., Santos, J.L., Chelysheva, L.,**
675 **Copenhaver, G.P., Horlow, C., and Mercier, R.** (2012). FANCM Limits Meiotic
676 Crossovers. *Science* **336**: 1588–1590.
- 677 **Darrier, B., Rimbart, H., Balfourier, F., Pingault, L., Josselin, A.-A., Servin, B., Navarro, J.,**
678 **Choulet, F., Paux, E., and Sourdille, P.** (2017). High-Resolution Mapping of Crossover
679 Events in the Hexaploid Wheat Genome Suggests a Universal Recombination Mechanism.
680 *Genetics* **206**: 1373–1388.
- 681 **Desai, A., Chee, P.W., Rong, J., May, O.L., and Paterson, A.H.** (2006). Chromosome
682 structural changes in diploid and tetraploid A genomes of *Gossypium*. *Genome* **49**: 336–
683 345.
- 684 **Dreissig, S., Maurer, A., Sharma, R., Milne, L., Flavell, A.J., Schmutzer, T., and Pillen, K.**
685 (2020). Natural variation in meiotic recombination rate shapes introgression patterns in
686 intraspecific hybrids between wild and domesticated barley. *New Phytologist* **228**: 1852–
687 1863.
- 688 **Durand, S., Lian, Q., Jing, J., Ernst, M., Grelon, M., Zwicker, D., and Mercier, R.** (2022).
689 Joint control of meiotic crossover patterning by the synaptonemal complex and HEI10
690 dosage. *Nature Communications* **13**: 5999.

- 691 **Edger, P.P., Smith, R., McKain, M.R., Cooley, A.M., Vallejo-Marin, M., Yuan, Y., Bewick,**
692 **A.J., Ji, L., Platts, A.E., Bowman, M.J., Childs, K.L., Washburn, J.D., Schmitz, R.J.,**
693 **Smith, G.D., Pires, J.C., and Puzey, J.R.** (2017). Subgenome Dominance in an
694 Interspecific Hybrid, Synthetic Allopolyploid, and a 140-Year-Old Naturally Established
695 Neo-Allopolyploid Monkeyflower. *The Plant Cell* **29**: 2150–2167.
- 696 **East, E.M.** (1933) The behavior of a triploid in *Nicotiana tabacum* L. *American Journal of*
697 *Botany*. 20:4:269–289
- 698 **Facon, M., Deniot, G., Lodé-Taburel, M., Archambeau, H., Montes, E., Dello, Y., Maillet,**
699 **L., Chèvre, A.-M., and Rousseau-Gueutin, M.** (2023). Why old duplicated genes are not
700 thrown away in (paleo)polyploids? Example from the *petC* gene in *Brassica napus*. *Plant*
701 *Molecular Biology* **113**: 323–327.
- 702 **Fernandes, J. B., Naish, M., Lian, Q., Burns, R., Tock, A. J., Rabanal, F. A., Wlodzimierz,**
703 **P., Habring, A., Nicholas, R. E., Weigel, D., Mercier, R., & Henderson, I. R.** (2024).
704 Structural variation and DNA methylation shape the centromere-proximal meiotic
705 crossover landscape in *Arabidopsis*. *Genome biology*, 25(1), 30.
- 706 **Gauthier, F., Martin, O.C., and Falque, M.** (2011). CODA (crossover distribution analyzer):
707 Quantitative characterization of crossover position patterns along chromosomes. *BMC*
708 *Bioinformatics* **12**: 27.
- 709 **Girard, C., Chelysheva, L., Choinard, S., Froger, N., Macaisne, N., Lehmemdi, A., Mazel,**
710 **J., Crismani, W., and Mercier, R.** (2015). AAA-ATPase FIDGETIN-LIKE 1 and Helicase
711 FANCM Antagonize Meiotic Crossovers by Distinct Mechanisms. *PLOS Genetics* **11**:
712 e1005369.
- 713 **de Givry, S., Bouchez, M., Chabrier, P., Milan, D., and Schiex, T.** (2005). Carhta Gene:
714 multipopulation integrated genetic and radiation hybrid mapping. *Bioinformatics* **21**: 1703–
715 1704.
- 716 **Goel, M., Sun, H., Jiao, W. B., and Schneeberger, K.** (2019). SyRI: finding genomic
717 rearrangements and local sequence differences from whole-genome assemblies. *Genome*
718 *biology*, 20(1), 277.
- 719 **Higo, H., Tahir, M., Takashima, K., Miura, A., Watanabe, K., Tagiri, A., Ugaki, M.,**
720 **Ishikawa, R., Eiguchi, M., Kurata, N., Sasaki, T., Richards, E., Takano, M., Kishimoto,**
721 **N., Kakutani, T., and Habu, Y.** (2012). DDM1 (Decrease in DNA Methylation) genes in
722 rice (*Oryza sativa*). *Molecular Genetics and Genomics* **287**: 785–792.
- 723 **Howell, E.C., Barker, G.C., Jones, G.H., Kearsey, M.J., King, G.J., Kop, E.P., Ryder, C.D.,**
724 **Teakle, G.R., Vicente, J.G., and Armstrong, S.J.** (2002). Integration of the Cytogenetic
725 and Genetic Linkage Maps of *Brassica oleracea*. *Genetics* **161**: 1225–1234.
- 726 **Jahier J, AM Chèvre, R Delourme, F Eber, AM Tanguy.** (1992). Techniques de cytogénétique
727 végétale, techniques et pratiques. INRA Editions, Paris.

- 728 **Kearsey, M.J., Ramsay, L.D., Jennings, D.E., Lydiate, D.J., Bohuon, E.J.R., and Marshall,**
729 **D.F.** (1996). Higher recombination frequencies in female compared to male meioses in
730 *Brassica oleracea*. *Theoretical and Applied Genetics* **92**: 363–367.
- 731 **Kosambi, D.D.** (1943). The estimation of map distances from recombination values. *Annals of*
732 *Eugenics* **12**: 172–175.
- 733 **Krug, C.A. and Mendes, A.J.T.** (1940). Cytological observations in *Coffea*. IV. *Journal of*
734 *Genetics* **39**: 189–203.
- 735 **Krzywinski, M., Schein, J., Birol, I., Connors, J., Gascoyne, R., Horsman, D., Jones, S.J.,**
736 **and Marra, M.A.** (2009). CircoS: An information aesthetic for comparative genomics.
737 *Genome Research* **19**: 1639–1645.
- 738 **Książczyk, T., Kovarik, A., Eber, F., Huteau, V., Khaitova, L., Tesarikova, Z., Coriton, O.,**
739 **and Chèvre, A.-M.** (2011). Immediate unidirectional epigenetic reprogramming of NORs
740 occurs independently of rDNA rearrangements in synthetic and natural forms of a polyploid
741 species *Brassica napus*. *Chromosoma* **120**: 557–571.
- 742 **Lambing, C., Kuo, P. C., Tock, A. J., Topp, S. D., and Henderson, I. R.** (2020). ASY1 acts as
743 a dosage-dependent antagonist of telomere-led recombination and mediates crossover
744 interference in *Arabidopsis*. *Proceedings of the National Academy of Sciences of the United*
745 *States of America*, 117(24), 13647–13658.
- 746 **Leflon, M., Eber, F., Letanneur, J.C., Chelysheva, L., Coriton, O., Huteau, V., Ryder, C.D.,**
747 **Barker, G., Jenczewski, E., and Chèvre, A.M.** (2006). Pairing and recombination at
748 meiosis of *Brassica rapa* (AA) × *Brassica napus* (AACC) hybrids. *Theoretical and Applied*
749 *Genetics* **113**: 1467–1480.
- 750 **Leflon, M., Grandont, L., Eber, F., Huteau, V., Coriton, O., Chelysheva, L., Jenczewski, E.,**
751 **and Chèvre, A.-M.** (2010). Crossovers Get a Boost in *Brassica* Allotriploid and
752 Allotetraploid Hybrids. *The Plant Cell* **22**: 2253–2264.
- 753 **Leitch, A. R. and Leitch, I. J.** (2008). Genomic plasticity and the diversity of polyploid plants.
754 *Science*, 320(5875), 481–483.
- 755 **Lenormand, T. and Dutheil, J.** (2005). Recombination difference between sexes: A role for
756 haploid selection. *PLoS Biology* **3**: 0396–0403.
- 757 **Lian, Q., Solier, V., Walkemeier, B., Durand, S., Huettel, B., Schneeberger, K., and**
758 **Mercier, R.** (2022). The megabase-scale crossover landscape is largely independent of
759 sequence divergence. *Nature Communications* **13**: 3828.
- 760 **Marand, A.P., Jansky, S.H., Zhao, H., Leisner, C.P., Zhu, X., Zeng, Z., Crisovan, E.,**
761 **Newton, L., Hamernik, A.J., Veilleux, R.E., Buell, C.R., and Jiang, J.** (2017). Meiotic
762 crossovers are associated with open chromatin and enriched with Stowaway transposons in
763 potato. *Genome Biology* **18**: 203.
- 764 **Martinez-Perez, E., and Moore, G.** (2008). To check or not to check? The application of
765 meiotic studies to plant breeding. *Current opinion in plant biology*, 11(2), 222–227.

- 766 **McKinley, K.L. and Cheeseman, I.M.** (2016). The molecular basis for centromere identity and
767 function. *Nature Reviews Molecular Cell Biology* **17**: 16–29.
- 768 **Melamed-Bessudo, C. and Levy, A.A.** (2012). Deficiency in DNA methylation increases
769 meiotic crossover rates in euchromatic but not in heterochromatic regions in *Arabidopsis*.
770 *Proceedings of the National Academy of Sciences* **109**: E981–E988.
- 771 **Mercier, R., Mézard, C., Jenczewski, E., Macaisne, N., and Grelon, M.** (2015). The
772 *Molecular Biology of Meiosis in Plants*. *Annu. Rev. Plant Biol.* **66**: 297–327.
- 773 **Naish, M., Alonge, M., Wlodzimierz, P., Tock, A. J., Abramson, B. W., Schmäcker, A.,**
774 **Mandáková, T., Jamge, B., Lambing, C., Kuo, P., Yelina, N., Hartwick, N., Colt, K.,**
775 **Smith, L. M., Ton, J., Kakutani, T., Martienssen, R. A., Schneeberger, K., Lysak, M.**
776 **A., Berger, F., Bousios, A., Michael, T. P., Schatz, M. C., and Henderson, I. R.**
777 (2021). The genetic and epigenetic landscape of the *Arabidopsis* centromeres. *Science*,
778 *374*(6569), eabi7489.
- 779 **Park, H.R., Park, J.E., Kim, J.H., Shin, H., Yu, S.H., Son, S., Yi, G., Lee, S.-S., Kim, H.H.,**
780 **and Huh, J.H.** (2020). Meiotic Chromosome Stability and Suppression of Crossover
781 Between Non-homologous Chromosomes in *xBrassicoraphanus*, an Intergeneric
782 Allotetraploid Derived From a Cross Between *Brassica rapa* and *Raphanus sativus*. *Frontiers*
783 *in Plant Science* **11**.
- 784 **Pecinka, A., Fang, W., Rehmsmeier, M., Levy, A.A., and Mittelsten Scheid, O.** (2011).
785 Polyploidization increases meiotic recombination frequency in *Arabidopsis*. *BMC Biology*
786 **9**: 24.
- 787 **Pelé, A., Falque, M., Trotoux, G., Eber, F., Nègre, S., Gilet, M., Huteau, V., Lodé, M.,**
788 **Jousseume, T., Dechaumet, S., Morice, J., Poncet, C., Coriton, O., Martin, O.C.,**
789 **Rousseau-Gueutin, M., and Chèvre, A.M.** (2017). Amplifying recombination genome-
790 wide and reshaping crossover landscapes in Brassicas. *PLOS Genetics* **13**: e1006794.
- 791 **Pelé, A., Rousseau-Gueutin, M., and Chèvre, A.-M.** (2018). Speciation Success of Polyploid
792 Plants Closely Relates to the Regulation of Meiotic Recombination. *Frontiers in Plant*
793 *Science* **9**, 907.
- 794 **R Core Team** (2021). R: A language and environment for statistical computing. R Foundation
795 for Statistical Computing, Vienna, Austria. URL <https://www.R-project.org/>. **Raz, A.,**
796 **Dahan-Meir, T., Melamed-Bessudo, C., Leshkowitz, D., and Levy, A.A.** (2021).
797 Redistribution of Meiotic Crossovers Along Wheat Chromosomes by Virus-Induced Gene
798 Silencing. *Front. Plant Sci.* **11**: 1–13.
- 799 **Rick, C.M., Chetelat, R.T., and DeVerna, J.W.** (1988). Recombination in sesquidiploid
800 hybrids of *Lycopersicon esculentum* × *Solanum lycopersicoides* and derivatives. *Theoretical*
801 *and Applied Genetics* **76**: 647–655.
- 802 **Rousseau-Gueutin, M., Belser, C., Da Silva, C., Richard, G., Istace, B., Cruaud, C.,**
803 **Falentin, C., Boideau, F., Boutte, J., Delourme, R., Deniot, G., Engelen, S., Ferreira de**
804 **Carvalho, J., Lemainque, A., Maillet, L., Morice, J., Wincker, P., Denoeud, F., Chèvre,**

- 805 **A.M., and Aury, J.M.** (2020). Long-read assembly of the Brassica napus reference genome
806 Darmor-bzh. *GigaScience* **9**: gaa137.
- 807 **Rowan, B. A., Heavens, D., Feuerborn, T. R., Tock, A. J., Henderson, I. R., and Weigel, D.**
808 (2019). An Ultra High-Density *Arabidopsis thaliana* Crossover Map That Refines the
809 Influences of Structural Variation and Epigenetic Features. *Genetics*, *213*(3), 771–787.
- 810 **Sardell, J.M. and Kirkpatrick, M.** (2020). Sex Differences in the Recombination Landscape.
811 *The American Naturalist* **195**: 361–379.
- 812 **Séguéla-Arnaud, M., Crismani, W., Larchevêque, C., Mazel, J., Froger, N., Choinard, S.,**
813 **Lemhemdi, A., Macaisne, N., Van Leene, J., Gevaert, K., De Jaeger, G., Chelysheva,**
814 **L., and Mercier R.** (2015). Multiple mechanisms limit meiotic crossovers: TOP3 α and two
815 BLM homologs antagonize crossovers in parallel to FANCM. *Proceedings of the National*
816 *Academy of Sciences* **112**: 4713–4718.
- 817 **Serra, H., Lambing, C., Griffin, C.H., Topp, S.D., Nageswaran, D.C., Underwood, C.J.,**
818 **Ziolkowski, P.A., Séguéla-Arnaud, M., Fernandes, J.B., Mercier, R., and Henderson,**
819 **I.R.** (2018). Massive crossover elevation via combination of HEI10 and recq4a recq4b
820 during *Arabidopsis* meiosis. *Proceedings of the National Academy of Sciences*. **115**: 2437–
821 2442.
- 822 **Siles, L., Hassall, K.L., Sanchis Gritsch, C., Eastmond, P.J., and Kurup, S.** (2021).
823 Uncovering Trait Associations Resulting in Maximal Seed Yield in Winter and Spring
824 Oilseed Rape. *Frontiers in Plant Science* **12**.
- 825 **Singh, D. K., Gamboa, R. S., Singh, A. K., Walkemeier, B., Van Leene, J., De Jaeger, G.,**
826 **Siddiqi, I., Guerois, R., Crismani, W., and Mercier, R.** (2023). The FANCC-FANCE-
827 FANCF complex is evolutionarily conserved and regulates meiotic recombination.
828 *Nucleic acids research*, *51*(6), 2516–2528.
- 829 **Suay, L., Zhang, D., Eber, F., Jouy, H., Lodé, M., Huteau, V., Coriton, O., Szadkowski, E.,**
830 **Leflon, M., Martin, O.C., Falque, M., Jenczewski, E., Paillard, S., and Chèvre, A.M.**
831 (2014). Crossover rate between homologous chromosomes and interference are regulated by
832 the addition of specific unpaired chromosomes in Brassica. *New Phytologist* **201**: 645–656.
- 833 **Tayalé, A., and Parisod, C.** (2013). Natural pathways to polyploidy in plants and consequences
834 for genome reorganization. *Cytogenetic and genome research*, *140*(2-4), 79–96.
- 835 **Tourrette, E., Falque, M., and Martin, O.C.** (2021). Enhancing backcross programs through
836 increased recombination. *Genetics Selection Evolution* **53**: 25.
- 837 **Underwood, C.J., Choi, K., Lambing, C., Zhao, X., Serra, H., Borges, F., Simorowski, J.,**
838 **Ernst, E., Jacob, Y., Henderson, I.R., and Martienssen, R.A.** (2018). Epigenetic
839 activation of meiotic recombination near *Arabidopsis thaliana* centromeres via loss of
840 H3K9me2 and non-CG DNA methylation. *Genome Research* **28**: 519–531.
- 841 **Vardi, A. and Zohary, D.** (1967). Introgression in wheat via triploid hybrids. *Heredity* **22**: 541–
842 560.

- 843 **Vincenten, N., Kuhl, L.-M., Lam, I., Oke, A., Kerr, A.R., Hochwagen, A., Fung, J., Keeney,**
844 **S., Vader, G., and Marston, A.L.** (2015). The kinetochore prevents centromere-proximal
845 crossover recombination during meiosis. *eLife* **4**: e10850.
- 846 **Wan, H., Li, J., Ma, S., Yang, F., Chai, L., Liu, Z., Wang, Q., Pu, Z., and Yang, W.** (2022).
847 Allopolyploidization increases genetic recombination in the ancestral diploid D genome
848 during wheat evolution. *The Crop Journal* **10**: 743–753.
- 849 **Wang, J., Lin, M., Crenshaw, A., Hutchinson, A., Hicks, B., Yeager, M., Berndt, S., Huang,**
850 **W.-Y., Hayes, R.B., Chanock, S.J., Jones, R.C., and Ramakrishnan, R.** (2009). High-
851 throughput single nucleotide polymorphism genotyping using nanofluidic Dynamic Arrays.
852 *BMC Genomics* **10**: 561.
- 853 **Wang, X., Wang, H., Wang, J., Sun, R., Wu, J., Liu, S., Bai, Y., Mun, J. H., Bancroft, I.,**
854 **Cheng, F., Huang, S., Li, X., Hua, W., Wang, J., Wang, X., Freeling, M., Pires, J. C.,**
855 **Paterson, A. H., Chalhouh, B., Wang, B., ... Brassica rapa Genome Sequencing**
856 **Project Consortium** (2011). The genome of the mesopolyploid crop species *Brassica*
857 *rapa*. *Nature genetics*, *43*(10), 1035–1039.
- 858 **Wang, Y. and Copenhaver, G.P.** (2018). Meiotic Recombination: Mixing It Up in Plants. *Annu.*
859 *Rev. Plant Biol.* **69**: 577–609.
- 860 **Yang, F., Wan, H., Li, J., Wang, Q., Yang, N., Zhu, X., Liu, Z., Yang, Y., Ma, W., Fan, X.,**
861 **Yang, W., and Zhou, Y.** (2022). Pentaploidization Enriches the Genetic Diversity of
862 Wheat by Enhancing the Recombination of AB Genomes. *Frontiers in plant science*, *13*,
863 883868.
- 864 **Yarnell, S.H.** (1931). A study of certain polyploid and aneuploid forms in *Fragaria*. *Genetics* **16**:
865 455–489.
- 866 **Yelina, N.E., Choi, K., Chelysheva, L., Macaulay, M., de Snoo, B., Wijnker, E., Miller, N.,**
867 **Drouaud, J., Grelon, M., Copenhaver, G.P., Mezard, C., Kelly, K.A., and Henderson,**
868 **I.R.** (2012). Epigenetic Remodeling of Meiotic Crossover Frequency in *Arabidopsis thaliana*
869 DNA Methyltransferase Mutants. *PLOS Genetics* **8**: e1002844.
- 870 **Zhang, L., Cai, X., Wu, J., Liu, M., Grob, S., Cheng, F., Liang, J., Cai, C., Liu, Z., Liu, B.,**
871 **Wang, F., Li, S., Liu, F., Li, X., Cheng, L., Yang, W., Li, M.H., Grossniklaus, U.,**
872 **Zheng, H., and Wang, X.** (2018). Improved *Brassica rapa* reference genome by single-
873 molecule sequencing and chromosome conformation capture technologies. *Horticulture*
874 *Research* **5**: 50.
- 875 **Zhang, T., Zhao, S. H., Wang, Y., and He, Y.** (2023). FIGL1 coordinates with dosage-sensitive
876 BRCA2 in modulating meiotic recombination in maize. *J. Integr. Plant Biol.* **65**: 2107–2121.
- 877 **Ziolkowski, P. A., Berchowitz, L. E., Lambing, C., Yelina, N. E., Zhao, X., Kelly, K. A.,**
878 **Choi, K., Ziolkowska, L., June, V., Sanchez-Moran, E., Franklin, C., Copenhaver, G.**
879 **P., and Henderson, I. R.** (2015). Juxtaposition of heterozygous and homozygous regions
880 causes reciprocal crossover remodelling via interference during *Arabidopsis* meiosis. *eLife*,
881 *4*, e03708.

882 **Ziolkowski, P.A., Underwood, C.J., Lambing, C., Martinez-Garcia, M., Lawrence, E.J.,**
883 **Ziolkowska, L., Griffin, C., Choi, K., Franklin, F.C.H., Martienssen, R.A., and**
884 **Henderson, I.R.** (2017). Natural variation and dosage of the HEI10 meiotic E3 ligase
885 control Arabidopsis crossover recombination. *Genes & Development* **31**: 306–317.
886

887

888 **List of Tables**

889 Table 1: Meiotic behavior, pollen fertility and seed set of the hybrids used in this study

890 Table 2: Characterization of the hybrids and segregating populations

891

892 **List of Supplementary Tables**

893 Table S1: Sequences of the KASPar markers used

894 Table S2: Genotyping data used to generate the generic maps

895 Table S3: HEI10 foci quantification used for Figure 4

896

897 **List of Figures**

898 Figure 1: Schematic representation of the production of the F1 and B1F1 hybrids and their
899 corresponding segregating backcross populations

900 Figure 2: Meiotic behavior on chromosome spreads in metaphase I in the different allotriploid
901 and allotetraploid hybrids using the C genome specific BoB014O06 probe

902 Figure 3: Immunolocalization of HEI10 and GISH-like labelling on diakinesis chromosomes in
903 pollen mother cells of the various allotriploid (a, b, c) and allotetraploid (d, e, f) hybrids

904 Figure 4: Average number of HEI10 foci per A bivalent in the hybrids

905 Figure 5: Homologous recombination landscape on the A genome of the six hybrids

906

907 **List of Supplementary Figures**

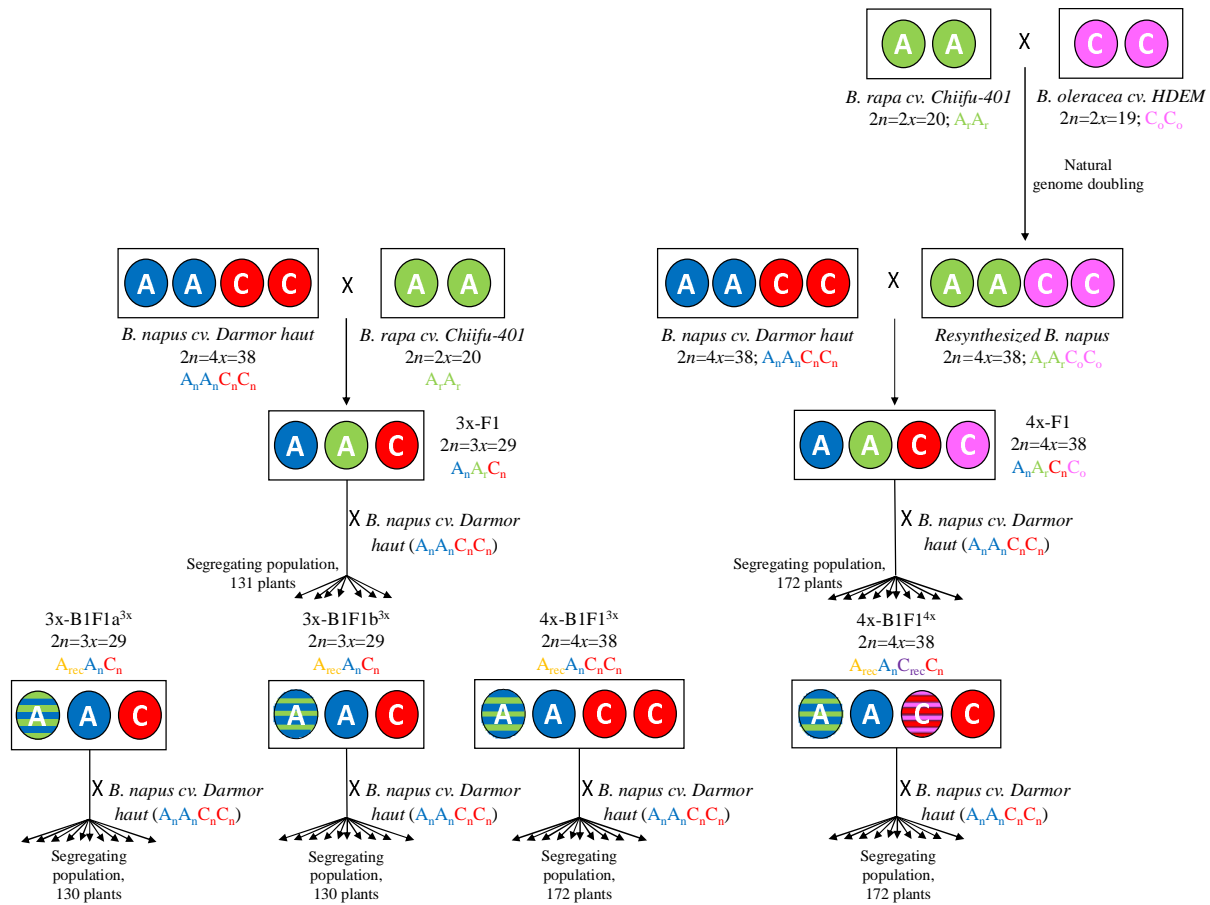
908 Figure S1: Improvement of the genome assembly of *B. napus* cv. Darmor

909

910

911

912



913

914

915 **Figure 1: Schematic representation of the production of the F1 and B1F1 hybrids and**
 916 **their corresponding segregating backcross populations.**

917 The names and the ploidy level of the parental lines are indicated and corresponds to *B. napus*
 918 cv. Darmor ($2n=4x=38$, $A_nA_nC_nC_n$), to *B. rapa* cv. Chiffu ($2n=2x=20$; A_rA_r) and *B. oleracea*
 919 cv HDEM ($2n=2x=18$; C_oC_o). The nomenclature A_r and A_n correspond to the A genome of *B.*
 920 *rapa* and *B. napus*, respectively, whereas C_o and C_n refer to the C genome of *B. oleracea* and
 921 *B. napus*, respectively. The index “rec” indicates that recombination occurred on the genome
 922 concerned. The allotriploid lineage is present on the left part of the diagram, while the right
 923 part corresponds to the allotetraploid lineage. The number of genotyped progenies for each of
 924 the six investigated segregating populations is indicated.

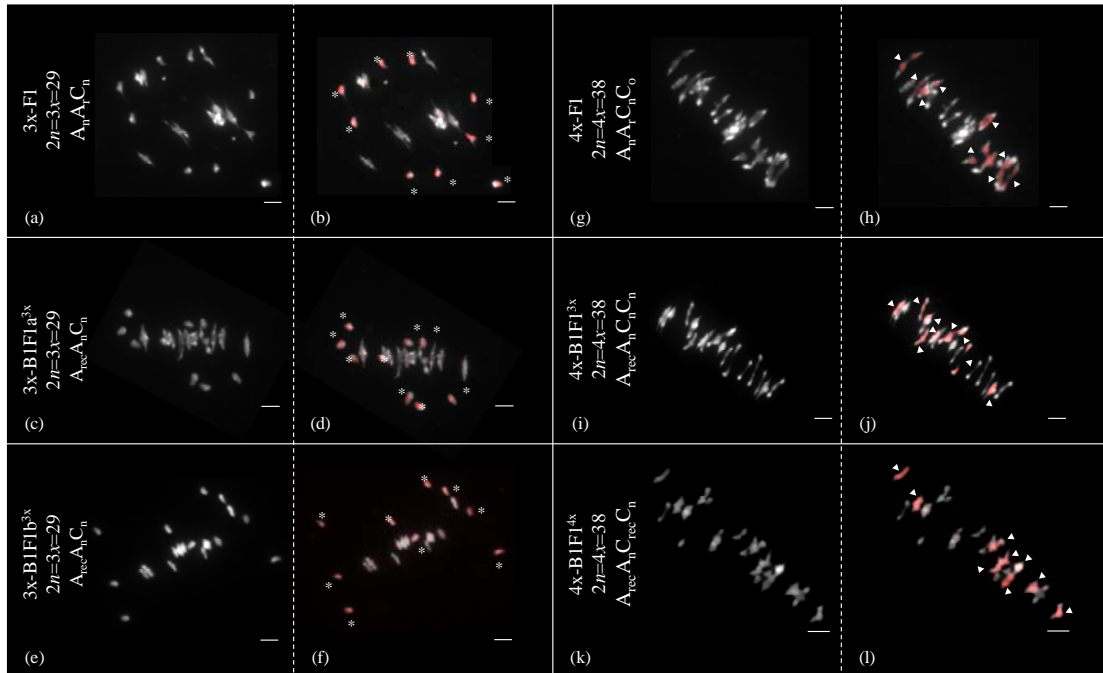
925

926 **Table 1: Meiotic behavior, pollen fertility and seed set of the hybrids used in this study.**

Hybrid	Genomic structure	Number of PMC	Meiotic behavior	Percentage of cells at the expected meiotic behavior	Pollen viability (%)	Average seed set per pollinated flower	References
3x-F1	$A_n A_r C_n$, $2n=3x=29$	21	9,38I+9,81II	81	68.80	2.26	Boideau et al. 2020
4x-F1	$A_n A_r C_n C_o$, $2n=4x=38$	20	0,2I+18,8II+0,05IV	85	96.70	10.16	Boideau et al. 2020
3x-B1F1a ^{3x}	$A_{rec} A_n C_n$, $2n=3x=29$	20	9I +10II	100	64.90	1.52	This study
3x-B1F1b ^{3x}	$A_{rec} A_n C_n$, $2n=3x=29$	20	9I+10II	100	61.40	1.49	This study
4x-B1F1 ^{3x}	$A_{rec} A_n C_n C_n$, $2n=4x=38$	17	0,2I+18,8II+0,05IV	85	93.80	13.22	This study
4x-B1F1 ^{4x}	$A_{rec} A_n C_{rec} C_n$, $2n=4x=38$	20	0.3I + 18.75II + 0.05IV	80	96.70	14.42	This study

927

928

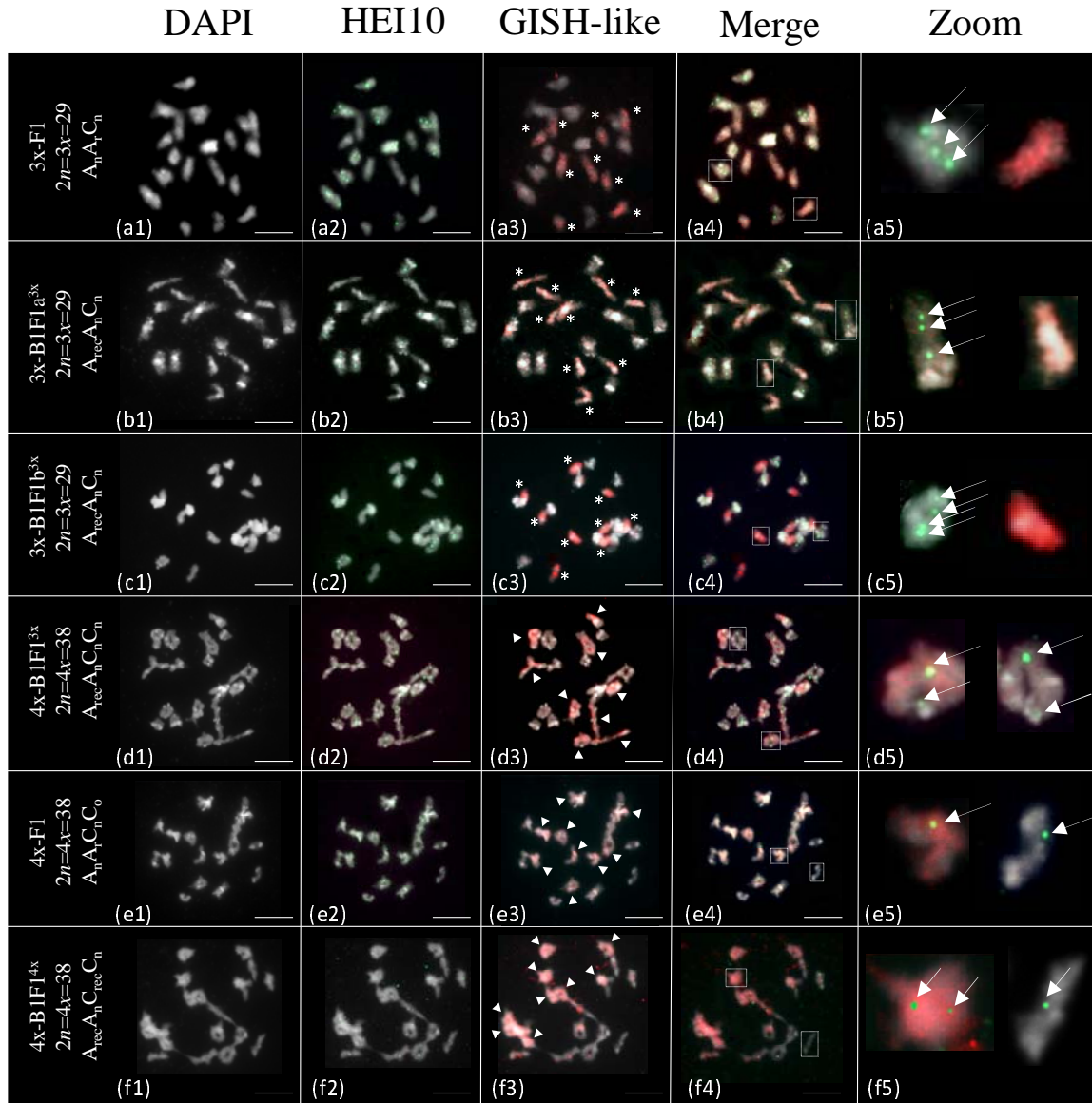


929

930 **Figure 2: Meiotic behavior on chromosome spreads in metaphase I in the different**
 931 **allotriploid and allotetraploid hybrids using the C genome specific BoB014O06 probe.**

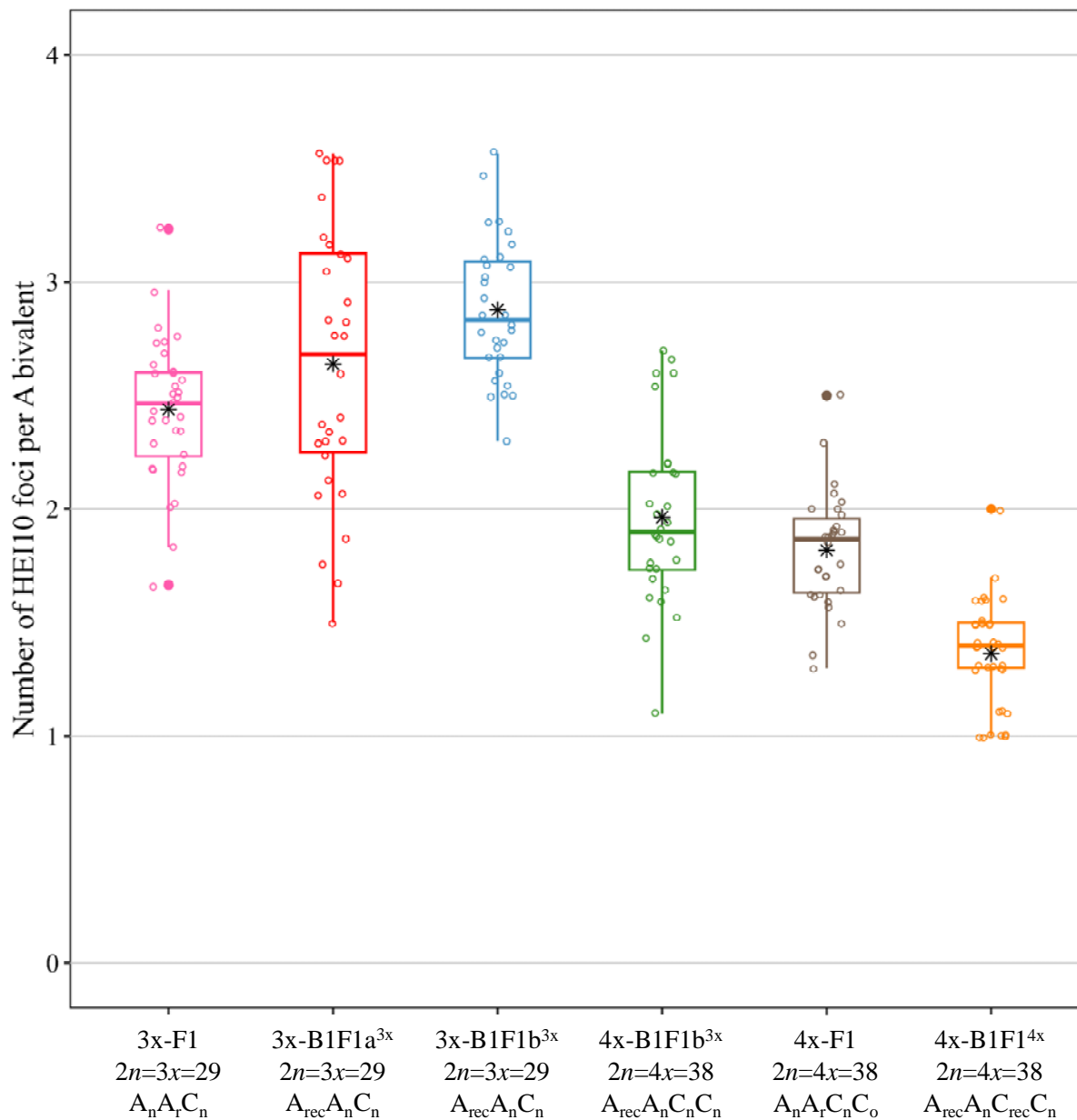
932 Chromosomes in grey are from the A-genome and chromosomes painted in red are from the
 933 C-genome. GISH-like analyses of meiotic chromosomes were carried out in the allotriploid
 934 (left) and allotetraploid (right) hybrids: 3x-F1 ($A_nA_rC_n$) (a-b), 3x-B1F1a^{3x} ($A_{rec}A_nC_n$) (c-d),
 935 3x-B1F1a^{3x} ($A_{rec}A_nC_n$) (e-f), 4x-F1 ($A_nA_rC_nC_o$) (g-h), 4x-B1F1^{3x} ($A_{rec}A_nC_nC_n$) (i-j), 4x-
 936 B1F1^{4x} ($A_{rec}A_nC_{rec}C_n$) (k-l). The nine C univalent in allotriploids (b, d, f) are indicated by
 937 stars, whereas the nine C bivalents in allotetraploids are shown with white arrows (h, j, l).
 938 Bars = 5µm. Original pictures from the 3x-F1 and 4x-F1 (a, b, g, h) derived from Boideau et
 939 al. 2021.

940



941 **Figure 3: Immunolocalization of HEI10 and GISH-like labelling on diakinesis chromosomes**
 942 **in pollen mother cells of the various allotriploid (a, b, c) and allotetraploid (d, e, f) hybrids.**

943 The investigated genotypes are: $3x-F1$ ($A_nA_rC_n$) (a), $3x-B1F1a^{3x}$ ($A_{rec}A_nC_n$) (b), $3x-B1F1b^{3x}$
 944 ($A_{rec}A_nC_n$) (c), $4x-B1F1^{3x}$ ($A_{rec}A_nC_nC_n$) (d), $4x-F1$ ($A_nA_rC_nC_o$) (e) and $4x-B1F1^{4x}$ ($A_{rec}A_nC_{rec}C_n$)
 945 (f). For each cell, chromosomes were counterstained with DAPI (white, a1-f1), HEI10
 946 immunolabeled (green, a2-f2) and red painted chromosomes derive from the C-subgenome
 947 (BoB014O06, a3-f3). The overlay of the three signals is shown in the column “Merge” (a4-f4)
 948 and a focus on some A and C chromosomes highlighted with a dotted white rectangle is
 949 displayed at the end of each rows in the column “Zoom” (a5-f5). In the third column, the nine C
 950 univalent chromosomes in the allotriploids are indicated by stars (a3, b3, c3) and the ten C
 951 bivalents in the allotetraploid hybrids are indicated by white arrow heads (d3, e3, f3). HEI10 foci
 952 are highlighted by white arrows in the last column (a5-f5). Bars = 5µm.



953

954 **Figure 4: Average number of HEI10 foci per A bivalent in the hybrids.**

955 The six investigated hybrids are as following: 3x-F1 ($A_nA_rC_n$), 3x-B1F1a^{3x} ($A_{rec}A_nC_n$), 3x-
 956 B1F1b^{3x} ($A_{rec}A_nC_n$), 4x-B1F1^{3x} ($A_{rec}A_nC_nC_n$), 4x-F1 ($A_nA_rC_nC_o$) and 4x-B1F1^{4x} ($A_{rec}A_nC_{rec}C_n$).

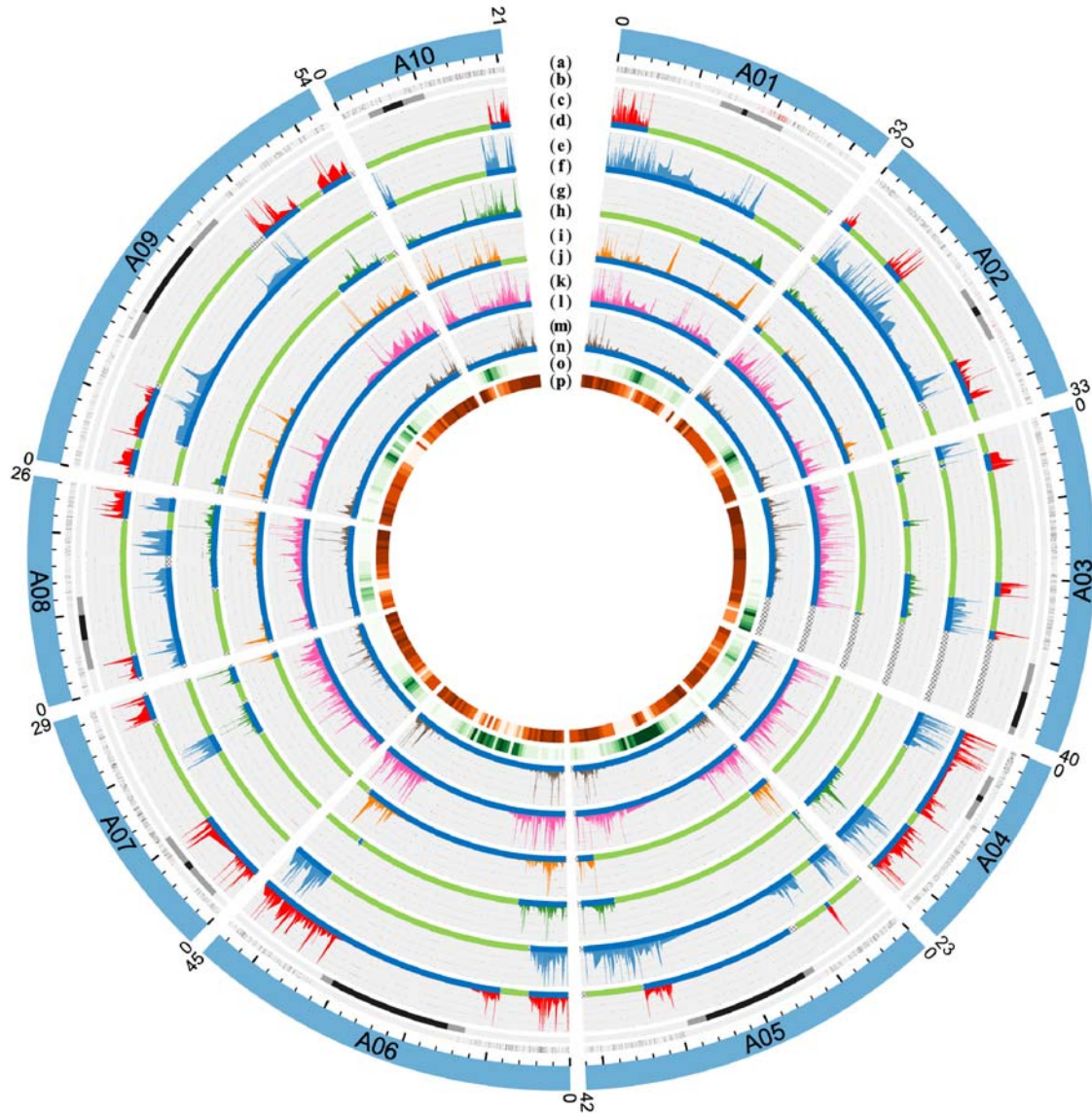
957 The means are indicated by a black asterisk.

958

959 **Table 2: Characterization of the hybrids and segregating populations.** For each hybrid
 960 and associated segregating population, several parameters are indicated. The star indicate that
 961 the F1 hybrid is fully heterozygous for the A subgenome

Hybrid	Genomic structure	Number of plants	Number of heterozygous regions	Number of polymorphic markers	Number of COs	Genetic size (cM)	Genome coverage (Mb)	Genome coverage (%)	Average recombination rate (cM/Mb)
3x-F1	$A_n A_r C_n$, $2n=3x=29$	131	10*	2274	3946	3045.3	327.58	94.55	9.30
3x-B1F1a ^{3x}	$A_{rec} A_n C_n$, $2n=3x=29$	130	22	980	2216	1739.7	146.68	42.33	11.86
3x-B1F1b ^{3x}	$A_{rec} A_n C_n$, $2n=3x=29$	130	18	1205	3365	2673.3	182.27	52.61	14.67
4x-B1F1 ^{3x}	$A_{rec} A_n C_n C_n$, $2n=4x=38$	172	17	1128	946	574.6	125.18	36.13	4.59
4x-F1	$A_n A_r C_n C_o$, $2n=4x=38$	172	10*	2274	1408	829.6	327.58	94.55	2.53
4x-B1F1 ^{4x}	$A_{rec} A_n C_{rec} C_n$, $2n=4x=38$	172	14	1099	1093	665.4	198.84	57.39	3.35

962



963
964 **Figure 5: Homologous recombination landscape on the A genome of the six hybrids.** The
965 first outer circle represents the ten A chromosomes from *B. napus* cv. Darmor-bzh. The second
966 circle represents the position of the polymorphic SNPs used to generate the genetic maps (a). The
967 red polymorphic SNPs on chromosomes A01 and A02 correspond to the pericentromeric KASPar
968 developed in this study. The third circle refers to the position of the pericentromeric and
969 centromeric regions in grey and black respectively (b). The lineplots correspond to the
970 recombination rates in the 3x-B1F1a^{3x} (c), 3x-B1F1b^{3x} (e), 4x-B1F1^{3x} (g), 4x-B1F1^{4x} (i), 3x-F1
971 (k) and 4x-F1 (m) hybrids. The genotyping blocks bellow each lineplot indicate that the region is
972 either heterozygous (blue) or homozygous (green) in the 3x-B1F1a^{3x} (d), 3x-B1F1b^{3x} (f), 4x-
973 B1F1^{3x} (h), 4x-B1F1^{4x} (j), 3x-F1 (l) and 4x-F1 (n) hybrids. The hatched areas (as example: end of
974 chromosome A03) correspond to regions without informative genotyping data. Finally, the two
975 most inner circles represent the transposable elements density (o) and gene density (p),
976 respectively.

977